JIMMA UNIVERSITY

JIMMA INSTITUTE OF TECHNOLOGY

FACULTY OF MATERIALS SCIENCE AND ENGINEERING

SUSTAINABLE SYNTHESIS AND CHARACTERIZATION OF NH_2-MIL-53(Al)/MIL-100(Fe) HETEROJUNCTIONS FOR VISIBLE LIGHT DRIVEN PHOTOCATALYTIC DEGRADATION OF RHODAMINE B DYE

BY

TEWODROS TEMTIME

A Thesis Submitted to Jimma University School of Graduate Studies in Partial Fulfillment of the Requirement in Master of Science Degree in Materials Science and Engineering.

June, 2024

Jimma, Ethiopa

JIMMA UNIVERSITY
JIMMA INSTITUTE OF TECHNOLOGY
FACULTY OF MATERIALS SCIENCE AND ENGINEERING
CHAIR OF MATERIALS SCIENCE AND ENGINEERING
MASTERS OF SCIENCE PROGRAM IN MATERIALS SCIENCE AND ENGINEERING

SYNTHESIS AND CHARACTERIZATION OF NH_2-MIL-53(Al)/MIL-100(Fe) HETEROJUNCTIONS FOR VISIBLE LIGHT DRIVEN PHOTOCATALYTIC DEGRADATION OF RHODAMINE B DYE

MAIN ADVISOR: Dr. SOLOMON DEMISS (PhD)
CO-ADVISOR: Dr. JEMAL MOHAMMED (PhD)

June, 2024
Jimma, Ethiopia

DECLARATION

I, Tewodros Temtime Yeshitla, proclaim that this, MSc thesis titled "**Sustainable Synthesis and Characterization of NH_2-MIL-53(Al)/MIL-100(Fe) Heterojunctions For Visible Light Driven Photocatalytic Degradation of Rhodamine B Dye**" is my own original work under supervision of Dr. Solomon Demiss and Dr. Jemal Mohammed and that no portion of this work referenced has not been submitted in to support an application for a different degree or certification either here or at any other university or academic institution. I confidentially Recognized in compliance with accepted reference guidelines, all work presented here is entirely my own.

	Name	Signature	Date
➢ Pricipal Investigator	_____	_____	_____
1. Chair person	_____	_____	_____
2. Main-Advisor	_____		_____
3. Co-Advisor	_____	_____	_____
4. External examiner	_____	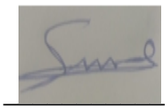	_____
5. Internal examiner	_____	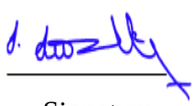	_____

ABSTRACT

Water pollution caused by toxic dyes from the textile industry has become a major concern nowadays. Specifically, rhodamine B (RhB) dyes found in textile wastewater have harmful and toxic impacts on the surroundings and human health. To address these problems, photocatalytic wastewater treatment using metal-organic frameworks (MOFs) and MOF-on-MOF heterojunctions has emerged as a promising and dynamic research area. This is due to the unthinkable properties of MOFs. However, pristine MOFs often have low photocatalytic efficiency due to their wide band gaps and high electron-hole recombination rates, which limits their practical application. Coupling two different MOFs into MOF-on-MOF heterojunctions can help overcome these limitations. The heterojunction structure facilitates precise charge transfer interfaces, thereby increasing the photocatalytic activity of the MOFs. Additionally, the heterojunction can preserve the porous framework of the MOF materials, supporting both adsorption and photocatalytic behaviors. This study describes the sustainable synthesis of pristine MIL-100(Fe) and NH_2-MIL-53(Al) MOFs, as well as the NH_2-MIL-53(Al)/MIL-100(Fe) heterojunctions. Characterization techniques such as X-ray diffraction (XRD), Fourier transform infrared (FT-IR) spectroscopy, Scanning electron microscopy (SEM), DRS-UV-vis spectroscopy (DRS-UV-vis) and so on were used to confirm the successful synthesis of the materials under environmentally friendly, energy-efficient, and economical (3E) conditions. The formation of the NH_2-MIL-53(Al)/MIL-100(Fe) heterojunctions significantly enhanced the photo-responsive range and charge separation efficiency, leading to improved photocatalytic activity in the degradation of RhB dye. Under visible light irradiation, the NH_2-MIL-53(Al)/MIL-100(Fe)-1wt% catalyst showed the highest performance, achieving 95.28% degradation efficiency within 140 minutes, outperforming the individual components. The active site trapping study revealed that superoxide radicals ($\bullet O_2^-$) and holes (h^+) play crucial roles in the photodegradation of RhB. Moreover, the selected photocatalyst revealed remarkable recyclability, retaining a high photocatalytic degradation efficency of 83.0% even after four cycles of activity.

Keywords: *Sustainable synthesis, MOF-on-MOF, Heterojunction, Photocatalysis*

ACKNOWLEDGEMENT

Firstly, I am grateful to the Heavenly GOD for blessing me with incredible resources, perseverance, and fortitude that allowed me to successfully complete this research project.

Secondly, I wanted to sincerely appreciate and show my gratitude to main-advisor Dr. Solomon Demiss, for his invaluable and long-lasting advice, as well as for sharing his expertise, experience, and knowledge in order to ensure the successful completion of this research project.

Thirdly, I want to express my deepest thanks to my co-advisor, Dr. Jemal Mohammed for his appropriate support from the start of this research project.

In addition, I want to express my deepest appreciation and gratitude to Materials Science and engineering department staffs specially my main-advisor Dr. Solomon Demiss for his patience, kindness, right encouragement from the beginning of this research work. Finally, my sincere thanks to Debre Berhan University, Chemistry staff's particularly for Ms. Bethelehem Teklu for her special support during laboratory work.

.

TABLE OF CONTENT

LIST OF FIGURES

List of Tables

ACRONYMS AND ABBRIVATIONS

AOPs	Advanced Oxidation Process
DRS-UV-vis	Diffuse Reflectance Ultra Violet visible Spectroscopy
FT-IR	Fourier Transformation Infrared Spectroscope
LMCT	Ligand-to-Metallic Charge-Transfer
MIL	Material of Institute Lavoisier
MOFs	Metal-Organic Frameworks
RhB	Rhodamine B
ROS	Reactive Oxygen Species
SEM	Scanning Electron Microscopy
UV-vis	Ultra Violet visible Spectroscopy
XRD	X-ray Diffraction

CHAPTER ONE

1. INTRODUCTION

1.1. General Background

In the last few decades, it have seen a marked decline in the quality of the world's water supplies due to the release of poisonous dyes into rivers, due to the rapid development of industrial activity and the excessive growth in global population. The presence of those toxic substances in the released industrial wastewater could seriously harm the surrounding area [1]. Especially the manufacturing process used in the textile industry (dying, bleaching, printing, and finishing) produce plenty of hazardous effluents. Xanthene dyes which are a class of organic dyes with a xanthene ring structure are most common effluents in wastewater due to their wide range of application in the industry, including biological staining, pH indicators, and fluorescent labeling. One of the organic dyes that exemplify the class of xanthene dyes is rhodamine B (RhB), due to its stable characteristics, quick coloring, and affordable price when compared to other industrial coloring reagents; it is frequently used for coloring in the fiber industry, laboratory staining, and cytological testing. Consequently, a significant amount of polluted wastewater specifically, RhB dye contaminated wastewater is released into the environment by those factories [2, 3]. Due to this, it has a significant adverse effects on the surroundings and human health, which causes cancer, obstruct sunlight's penetration, and harm aquatic life [4].

Significant advancements in the treatment of wastewater have been accomplished in the decreasing of dye pollution. wastewater which contains dye is treated using a variety of strategies, including chemical, physical, and biological methods [5]. The biological treatment approach is not cost-effective, and produces hazardous contaminants after the process, render the technique inefficient. Adsorption, filtration, and numerous other physical approaches are non-adverse methods that transfer contaminants from one phase to another. They might also create secondary contaminants that are certainly hazardous. In conventional chemical techniques the degradation of RhB dye also created hazardous byproducts. Thus, it's necessary to consider more environmentally benign techniques for pollutant degradation [5].

Auspiciously, employing photo-based advanced oxidation processes (AOPs) presents an achievable approach for addressing these concerns [2, 6]. AOPs is regarded as one of the most exciting advancements, because of its excessive performance, low cost, and simplicity [7]. As an environmentally friendly technique, photocatalysis offers numerous advantages, such as: it breaks down pollutants without the need for additional chemical compounds, like ozone; it operates within ambient conditions (only using catalyst, water and photon); and it converts hazardous natural effluents into harmless compounds like water and carbon dioxide[8]. The most widely used AOP method for generating reactive oxygen species (ROS) under light exposure is semiconductor photocatalysis. ROS has an ability to transform macromolecular organic contaminants into safe and innocuous by-products [9]. TiO_2, ZnO, Fe_2O_3, and so on, are examples of semiconductor catalysts which gained significant attention because of their wide range of application. Heterogeneous photocatalysis based on conventional semiconductor catalysts has many important benefits, while there are also certain inevitable limitations [10].

The design for novel photocatalysts with enhanced performance is a hot topic in several scientific domains, including material science, green chemistry, environmental science, etc. for state-of-the-art applications. An extensive interest has been shown in Metal-Organic Frameworks (MOFs), which are an innovative and elegant kind of porous crystalline hybrid material with unthinkable characteristics like a large specific surface area, a flexible composition, an open framework, and uniform but adjustable cavities. MOFs are formed by assembling metal ions or clusters (as a node) and using organic linkers as spacers. MOFs outperform conventional materials in various fields, including, gas storage and separation, adsorption, catalysis, and others, they are utilized as adsorbents and photocatalysts to remove and/or decompose organic contaminants from wastewater. MOFs are a green photocatalyst due to their hybrid framework structure with remarkable ligand-to-metallic charge-transfer (LMCT) transitions [11-13]

Among the numerous types of MOFs, MIL-100(Fe) has typically garnered a lot of interest for dye adsorption and photocatalysis due to high specific surface area[14] Nevertheless, the utilization of pristine MIL-100(Fe) in a single adsorption and/ or photocatalysis process often presents several challenges. Firstly, the adsorption equilibrium may prevent the pollutants from being entirely eliminated, secondly, the weak framework of the spent MIL-100(Fe) MOF makes its regeneration challenging, and thirdly, the higher charge carrier recombination led to reduce the photocatalytic activity[15]. To combat these challenges, coupling of MIL-100(Fe) MOF with other MOFs, semiconductor, metal nanoparticle, and so on is one of the possible strategies[16, 17]. A significant amount of research on the synthesis of semiconductor@MOF heterojunctions has been done in the past several years [18]. MOFs huge specific surface area enriches dyes and provides wide active sites for dye interaction with the photocatalyst. Therefore, a semiconductor@MOF heterojunction photocatalyst have superior purification capabilities than individual components under photocatalysis [19]. However, semiconductor@MOF effectively integrates adsorption and photocatalysis, several difficulties still exist, such as: (i) the way in which the outer layer MOF affects the semiconductor's light absorption performance (ii) the photocatalysts catalytic activity per unit mass is influenced by the amount of MOF in the shell; and (iii) some MOFs and semiconductors include heavy metals, which can pollute treated water bodies[9]. Consequently, additional optimization is needed.

MOF@MOF heterojunctions are used in a various applications, which includes adsorption and gas separation, catalysis, photocatalysis and sensing identification (including electrical and biosensing) [20, 21]. MOF@MOF provides a framework for the integrated adsorption and photocatalytic degradation of contaminants in water. The two MOF constituents demonstrated superior adsorption and photocatalytic properties, achieving the intended dual function synergy, all while utilizing a sustainable and recyclable methodology.

The MIL(Fe) MOF is one of the larger Fe-MOF family members with a shorter band gap with better photocatalytic performance [22]. Meanwhile, 3D porous crystalline NH_2-MIL-53(Al) is also very appealing for catalysis, photocatalysis and so on applications, due to their good stability, reasonable price, simple preparation, non-polluting properties of Al and suitable band gap[23]. Therefore, NH_2-MIL-53(Al) and MIL-100(Fe) have unique properties that, when used together, provide a synergistic impact for increased photocatalytic activity.

In regard to capacity for adsorption, the two MOFs' synergistic adsorption exhibited a pore channel restricted effect, in which it enhances the quantity of RhB adsorption and boosting RhB photocatalytic capabilities. Due to its large surface area, MIL-100(Fe) increases contact of RhB dye and photoactive catalytic sites and also it acts as a co-catalyst that synergistically boosts the photocatalytic activity of NH_2-MIL-53(Al).Additionally, the presence of amino functional groups (-NH_2) in NH_2-MIL-53(Al) offers extra active sites for interacting with RhB molecules. These amino groups have the ability to engage electrostatically and establish hydrogen bonds with RhB, which helps with its adsorption and subsequent photocatalytic degradation [23].

1.2. Statements of the Problem

The discharge of toxic dyes like rhodamine B (RhB), methyl orange, methyl blue and so on from numerous sectors has made water pollution a major problem in today's globe. These contaminants may originate from the textile, leather tanning, and electroplating industries' effluents. The organic dyes are extremely harmful, leading to various health issues including cancer [24]. The presence of those toxic substances in the released industrial wastewater could also seriously harm the surrounding area [1].

Especially the manufacturing process used in the textile industry (dying, bleaching, printing, and finishing) produce plenty of hazardous effluents. Xanthene dyes which are a class of organic dyes with a xanthene ring structure are most common effluents in wastewater due to their wide range of application in the industry, including biological staining, pH indicators, and fluorescent labeling. One organic dye that exemplifies the class of xanthene dyes is RhB dye. Due to its stable characteristics, quick coloring, and affordable price when compared to other industrial coloring reagents, it is frequently used for coloring in the fiber industry, laboratory staining, and cytological testing. consequently, a significant amount of polluted wastewater specifically, RhB dye contaminated wastewater is released into the aquatic environment by those factories [2, 3]. Due to this, it has a detrimental effect on the surrounding. It also have an adverse effect in human health by weaken the immune system, causing cancer and, so on [25].

Therefore, this study aimed to possibly finding cost effective, easily prepared and efficient solution for water related problems by developing high performance NH_2-MIL-53(Al)/MIL-100(Fe) heterojunction materials. In addition, use of this MOF-on-MOF heterojunction in photocatalytic application of dye degradation under light irradiation. The photocatalytic performance of the developed MOF-on-MOF photocatalyst was investigated using synthetic RhB dye solution. At the end of this research, it will add value in textile wastewater treatment process with providing a clean, eco-friend, flexible, cost effective, recyclable and sustainable MOF based photocatalyst.

1.3. Objective of Study

1.3.1. General Objective

The main objective of this study was to synthesize, characterize, and evaluate the photocatalytic capacity of NH_2-MIL-53(Al)/MIL-100(Fe) heterojunctions for the degradation of RhB dye under visible light irradiation.

1.3.2. Specific Objectives

- ☑ To synthesize NH_2-MIL-53(Al), MIL-100(Fe), and NH_2-MIL-53(Al)/MIL-100(Fe) materials using water as a sole solvent in an energy efficient way via precipitation method.
- ☑ To characterize the as-obtained samples using different physicochemical techniques.
- ☑ To apply the as-obtained samples in the photocatalytic degradation of RhB dye under visible light irradiation.
- ☑ To evaluate the stability of the NH_2-MIL-53(Al)/MIL-100(Fe) heterojunction.
- ☑ To apply efficient photocatalyst for RhB dye degradation under solar/ outdoor system.

1.4. Research Hypothesis

The sustainable synthesis and characterization of NH_2-MIL-53(Al)/MIL-100(Fe) heterojunctions was lead to a highly effective photocatalyst with excellent capacity in the degradation of toxic dyes. The synergistic interaction between NH_2-MIL-53(Al) and MIL-100(Fe) MOFs was enhanced the photocatalytic degradation compared to individual counter parts. The as-obtained pristine MOFs and heterojunction materials under sustainable conditions demonstrate well-defined morphologies and desirable physicochemical properties.

- ➢ The sustainable synthesis method was facilitated the successful formation of a NH_2-MIL-53(Al)/MIL-100(Fe) heterojunctions with enhanced physicochemical properties compared to the individual component.
- ➢ The NH_2-MIL-53(Al)/MIL-100(Fe) heterojunctions was exhibited better photocatalytic capacity in the degradation of RhB dye than NH_2-MIL-53(Al) and MIL-100(Fe) MOFs.
- ➢ The NH_2-MIL-53(Al)/MIL-100(Fe) heterojunction was demonstrated good reusability for 4^{th} cycles, indicating its practical applicability for wastewater treatment.

1.5. Significance of the Study

This research work introduces a novel design of MOF-on-MOF heterojunction nanocomposite materials by utilizing NH_2-MIL-53(Al) and MIL-100(Fe) MOFs and behaves as a photocatalyst. Currently, the MOF-based photocatalyst's was synthesized under sustainable approach within few hours, at room temperature and without the addition of any inorganic corrosive acid (HF, HNO_3, etc.) and toxic organic solvents (DMF), that is the major challenges of scientific community thus; this study can fill such kind of gaps, because this synthesis strategy quiet simple, reproducible, low cost and synthesized within 24 hour under environmental, energetic and economical system.

This novel MOF-based photocatalyst efficiently degrade RhB dye with low cost of activation energy (i.e. light irradiation). Furthermore, the following benefits obtained from the study:

- It aids technological progress in the field and helps to fill the research gap.
- It reduces the use of conventional water treatment methods and UV light in dye degradation process.
- The photocatalytic processes operation was designed to be more simple, recyclable, flexible, economically cheap and easily adaptable.
- It reduces the impacts of organic pollutants on water qualities.

This research work may create a linkage between University and textile industries to solve such kind of environmental problems.

1.6. Scopes of Study

This study focused on the sustainable synthesis and characterization of NH_2-MIL-53(Al)/MIL-100(Fe) heterojunctions, which is prepared sustainably using the precipitation method, and examining how effective it is as a photocatalyst in degrading harmful RhB dye which present in textile industrial effluent.

CHAPTER TWO

2. LITERATURE REVIEW

2.1. Wastewater Treatment

These days, industrial wastewater contamination is one of the world's top concerns. Treatments of industrial wastewater are essential for the health of people and the environment. Various techniques have been used to treat wastewater; the methods include coagulation, electrocoagulation, biocoagulation, plasma treatment, filtering, electrochemical treatment, biodegradation, evaporation, adsorption, and ion exchange. These can also be chemical, biological, or physical methods [26-28]. However, they have low productivity, high starting cost, high usage of energy, and also they have possibility of secondary contaminates that cause human diseases like mutations and cancer [29].

The advantages of semiconductor photocatalysis technology over other physicochemical techniques include its high efficiency, nontoxicity, and environmental friendliness. The photocatalytic process is a "green" purification technology since it can totally decompose organic contaminants into CO_2 and H_2O [30, 31]. It is well acknowledged that the primary obstacles impeding the advancement of semiconductor photocatalytic technology are the reduced solar energy usage efficiency and the charge carriers' rapid recombination[32]. Consequently, the finding of superior, effective, and long-lasting light responsive photocatalysts in visible light for the decomposition of contaminants continues to be a crucial but difficult research objective. In the field of photocatalysis, MOFs has attracted a lot of interest. [33].

2.2. Industrial Wastewater

Nowadays, the entire globe, especially the industrialized countries, is very concerned about environmental pollution brought on by industrial effluent. The following are some of the main causes of environmental pollution in general: energy consumption, radioactive waste, sewage and wastewater from industries, mining activities, pesticides and chemicals, fertilizers, urban development, and so on. Water utilized for residential, commercial, or agricultural purposes really pollutes because of the various chemicals used in the processes and the exposure of it to nearby microorganisms. There are three categories of water pollutants: chemical, microbiological, and radioactive.

Human health is negatively impacted by ingestion of these pollutants; pathogenic contaminants can often induce gastro interstitial illness, and chemical contaminants could also damage functioning systems of the vital organs[34]. The chemical contaminant also known as an organic contaminant, poses a risk to human health because of its inability to degrade due to the aromatic groups which are found in its structure [35]. Figure (2.1) below, provides an overview of the categories of water contaminants.

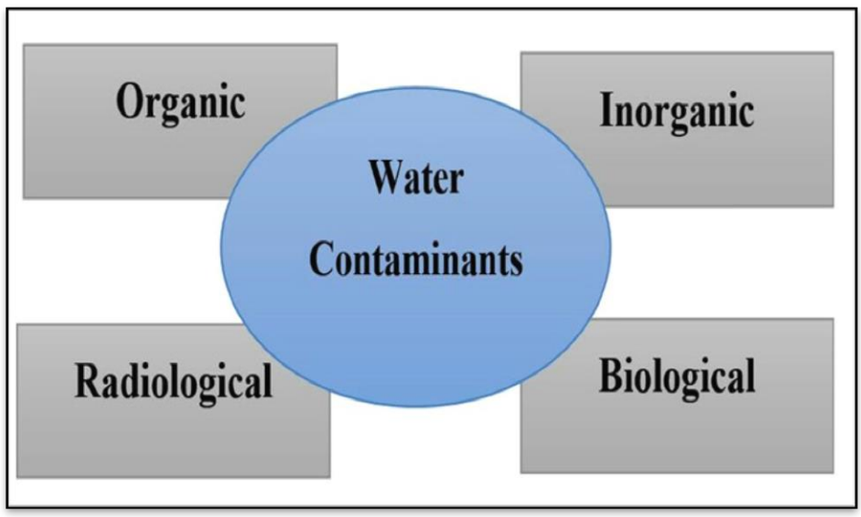

Figure 2.1.Types of water contaminants[36].

Among the organic pollutants produced by numerous industries, organic dyes which present in wastewater from industries are the major one. These contaminants may result in skin irritation, cancer, and mutations [37]. Additionally, they lower the water's oxygen content, which results in ecological issues [38]. The primary industries for dye release are particularly those in the textile sector.

2.2.1. Textile industries wastewater

The second-most water-polluting industry in the world is the textile industry [39]. About 20% of the pollution in clean water worldwide is caused by dyeing and finishing processes [40]. It consumes numerous volume of water approximately 425,000,000 gallons of water per day and use more than 20,000 different chemicals for their manufacturing processes such as bleaching, dyeing, printing and stiffening fabric products [41]. Each of these unit operations are highly water intensive and continuously discharges a huge volume of toxic wastewater in to water bodies. It potentially damages the aquatic ecosystem and brings some carcinogenic diseases on human and animal health. Some toxic compounds generated from each textile processing and their natures are given below in Figure (2.2)[42]. In the textile dyeing process an extensive amount of synthetic dyes are consumed and continuously discharges colored wastewater into the adjacent waterway, farming fields, irrigation channels, etc. These organic dyes have high chemical and photolytic stability due to that the different conventional treatment methods do not degrade the dyes found in textile wastewater effectively [43]. In addition to harming the aesthetics of the water bodies, textile dyes block light from penetrating the water, slowing photosynthesis and depleting oxygen in the water, which has an impact on the aquatic ecosystems overall [44].

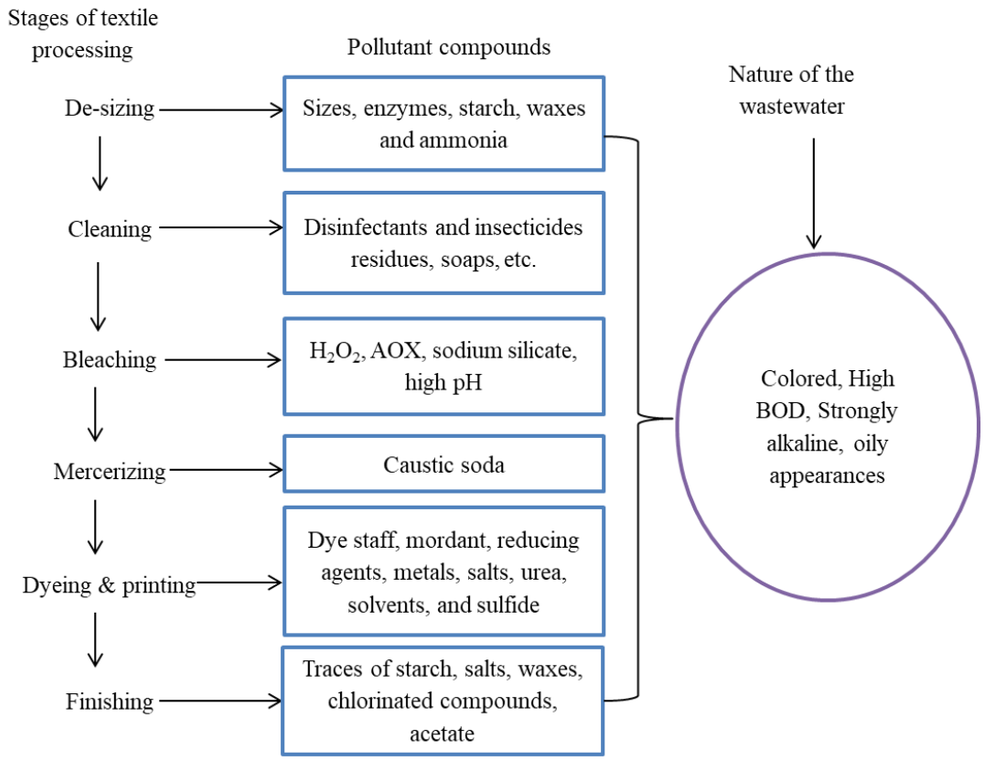

Figure 2.2. Possible pollutants from each stage of textile processes.

2.2.2. Rhodamine B Dye

RhB dye is xanthene based dye with a bright pink color. It is a positively charged basic dye with a chemical formula of $C_{28}H_{31}ClN_2O_3$. Because of its high water solubility, it can be dissolved in water to form an inert solution at room temperature. [45]. At room temperature, it is a solid, odorless, bright pink powder, which has a characteristic reddish-purple color in the oxidized state when it dissolved in water [46]. During dying process, about 90% of inputs (i.e. dyes, water and other organic chemicals) get discharged as effluents (Figure (2.3)) into natural water bodies [42]. Treatment of RhB dye containing wastewater before discharging into the environment is crucial solution to protect the limited water resource quality [47]. The three approaches physical, chemical, and biological methods are frequently utilized in wastewater treatment [48] The majority of treatment systems of waste water treatment are easy to operate, however they have disposal issues and are expensive.

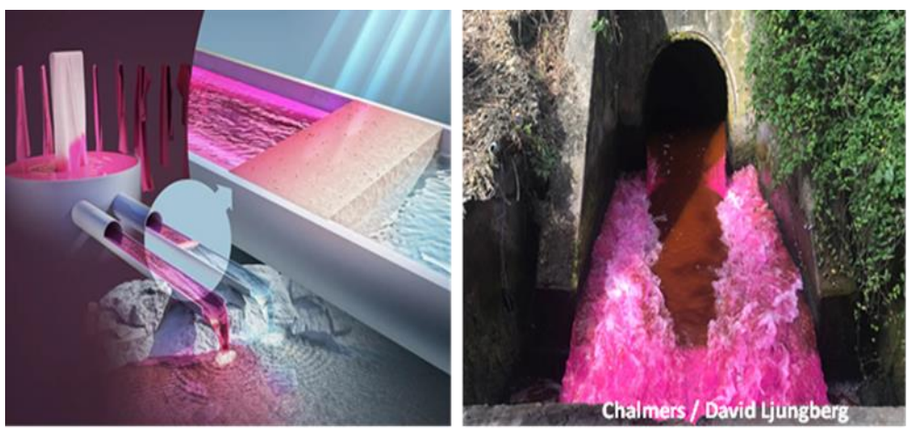

Figure 2.3. Water pollution by RhB color textile wastewater

2.3. Approaches for Treating Industrial Wastewater

An essential task for the preservation of environmental and human health is the treatment of industrial wastewater. Various techniques for purifying wastewater have been used, including chemical oxidation [27], biological degradation [34], and adsorption [52] and Photocatalysis. The pollutant simply moves from the phase of a liquid to the solid phase in most of these the conventional approaches, which is one of the drawbacks of some of these techniques. Adsorptive removal is a fast, highly effective, and reasonably priced wastewater treatment method. It is also simple to execute and less susceptible to harmful elements. A vast range of substances, including activated carbon, kaolin, mesoporous silica, agricultural wastes, and gelatin fiber, have been employed as adsorbents in recent years. These materials nonetheless have trouble separating in an aqueous solution, despite their similarities. However, adsorption may also block filters if done too frequently, even if it recycles and uses a lot of the carbonaceous material alone [52].

Photocatalysis which is one of the AOP seems to be an acceptable alternative technique; due to that the pollutant is entirely broken down into non-toxic inorganic compounds (CO_2 and H_2O) while using this method [5, 49, 50].AOPs have been utilized to degrade organic dyes for the past 30 years. Heterogeneous photocatalysis is one of the AOPs that is most frequently utilized since it requires mild temperature and pressure, complete mineralization of the pollutant, and no waste disposal [51, 52].

2.3.1. Common and advanced oxidation process

In the process of treating wastewater with coagulants either organic or inorganic hydrolyze pollutants that have been adsorbed on their surface to produce simple soluble products [28, 53, 54]. The effluent produced by the process is what causes Alzheimer’s disease. Another type of wastewater treatment method is filtration, which uses clay, membranes, or nanomaterial to separate impurities from water.However, filtration is ineffective in eliminating organic contaminants because of their chemical constitution [28, 54]. Degradation of organic dyes can be accomplished via ozonation, the Fenton reaction, and homogenous AOP. However, the Fenton approach produced secondary pollution like iron sludge, and the ozonation process uses a lot of electricity, which is costly [55, 56]. AOPs are extremely effective methods for decomposition of airborne and waterborne persistent organic and inorganic contaminants. These procedures produce reactive hydroxyl radicals (•OH) or other potent oxidizing species. Examples of these processes include ozone oxidation, Fenton's reagent, photo-Fenton, photocatalysis, electrochemical oxidation, and plasma-based approaches. Advantages of AOPs include their broad applicability, effectiveness in mineralizing contaminants, and capacity to handle intricate mixes. AOPs are critical to the effective and long-term remediation of contaminated settings and are indispensable in the fight against difficult pollutants [57]. Heterogeneous photocatalytic degradation technology, one of the AOPs has the advantages of low energy consumption, wide range a of applications, and moderate reaction conditions. It has been demonstrated to be highly effective at breaking down poisonous dyes into less harmful or easily biodegradable molecules when exposed to light, or even mineralizing them into safer substances like CO_2 and H_2O[58].

2.4. Photocatalysis Mechanism

The main energy source for photocatalytic processes is light energy, also known as photon energy. The electrons in the semiconductor's valence band are activated and move to the conduction band of the semiconducting material when photons of light energy equal to or greater than the semiconductor's band gap fall on it. When light energy equal to or greater than a catalyst's band gap is absorbed, electron (e-) and hole (h^+) pairs are produced. Moreover, the conduction band's e^- reacting with dissolved oxygen species produce the superoxide radical, whereas h^+ in the valance band reacting with water produce hydroxyl radicals. [34]. Hydroxide radical plays an important role in the degradation of organic pollutants [35]. The process by which h^+ generates hydroxyl ($\bullet OH^-$) ions and e^- produces superoxide ($\bullet O_2^-$) radicals is shown in Figure (2.4) below.

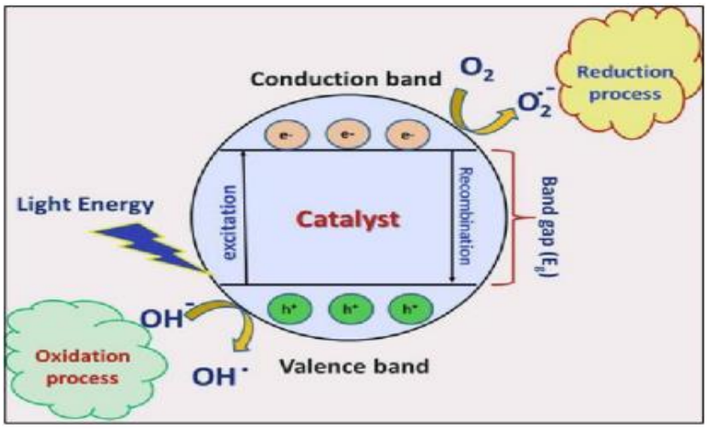

Figure 2.4. Schematic representation of photocatalysis mechanism [59]

2.4.1. Oxidation reaction

When light radiation causes an electron to transfer from the semiconductor's valence band to the conduction band, the semiconductor's surface absorbs water, which is oxidized and forms hydroxyl radicals during the wastewater treatment reaction. After that, because of the hydroxide radicals' ability to decompose organic materials, they react with the organic materials in the dyes. In the event that oxygen is available throughout the process, the intermediate organic molecules consume the dispersed oxygen, starting a radical chain reaction that ultimately results in the organic molecules breaking down into carbon dioxide and water as shown in Figure (2.5)[60].

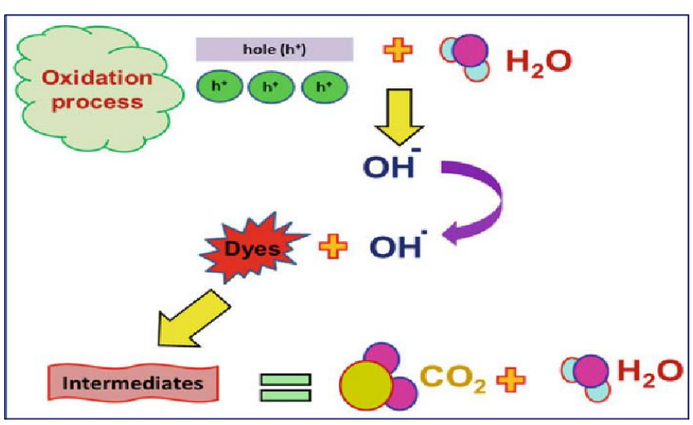

Figure 2.5. Schematic representation of oxidation processes [61].

2.4.2. Reduction reaction

In a reduction reaction, the reduction of oxygen occurs as dissolved oxygen molecules combine with conduction band electrons, resulting in the formation of superoxide radicals. The intermediate compounds created by oxidation processes are then reacted with by these superoxide radicals. Hydrogen peroxide or other peroxides are produced as a result of this reaction (Figure (2.6)).

Hydrogen peroxide decomposes over time and turns into water. This is a multi-step process wherein oxygen is first reduced, superoxide radicals are then attached to intermediate products, and peroxide or hydrogen peroxide is then converted into water. These reactions contribute to oxygen depletion, cellular damage, and pollutant breakdown, and they are important in many biological systems and environmental processes. In disciplines like chemistry, environmental science, and medicine, an understanding of these complex mechanisms is essential [62].

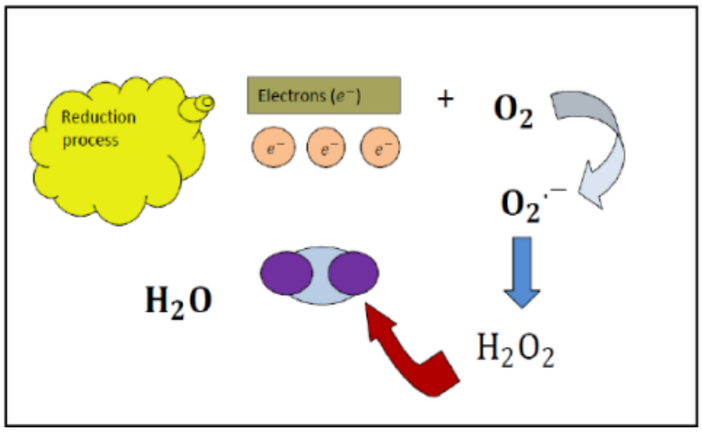

Figure 2.6. Schematic representation of reduction reaction [61].

2.5. MOF-Based Heterojunctions for Photocatalysis Application

A lot of interest has been focused on MOFs, a novel family of porous materials with enormous surface areas, open frameworks, uniform but adjustable cavities, and crystalline structures. It is created by assembling organic linkers and metal ions or clusters. MOFs outperform conventional materials in a number of applications, including catalysis,gas separation and storage. They are employed as adsorbents and photocatalysts to remove organic pollutants from water. MOF is an effective photocatalyst because of its transitional metal centers and organic linkers (Figure (2.7)), which produce distinct ligand-to-metal charge-transfer (LMCT) transitions [63-66].

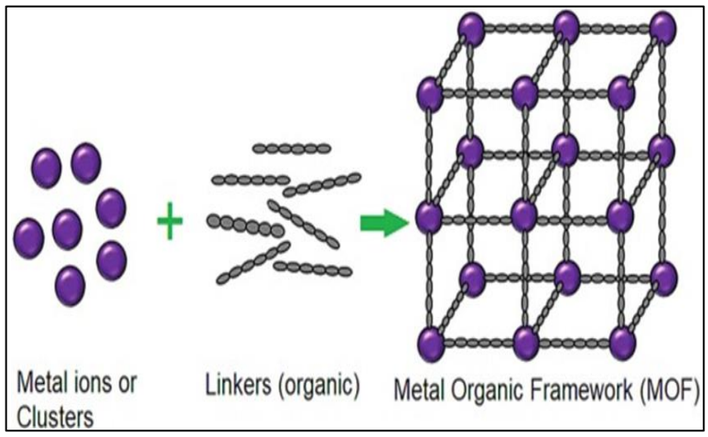

Figure 2.7. Schematic of Metal organic Framework (MOFs)[67].

Due to their specialized active sites, size and shape selectivity, synergistic effects, stability in challenging environments, photochemical and photocatalytic properties, chiral catalysis, catalyst support capabilities, gas separation and capture applications, environmental sustainability, computational design, and machine learning advancements, MOFs are highly effective catalysts. MOFs provide precise control over catalytic characteristics and a large number of active sites, enabling optimal performance. Size and shape selectivity is made possible by their porous structure, which improves specificity and efficiency. Catalytic activity is further enhanced by synergistic effects and stability under adverse conditions. Photo chemically active MOFs allow for energy-efficient catalysis, while chiral MOFs help enantioselective processes [68].

Pyrolysis has been the focus of current efforts to convert MOFs (as a precursor) into metal oxide nanoparticles. Precursors of ZnO and TiO_2 with improved photodegradation performances were created using MOFs based on zinc and MOFs based on titanium, such as MOF-5, Ti-benzene dicarboxylate (MIL-125(Ti)), and zeolite imidazolate framework-8 (ZIF-8). For example, Feng et al. prepared N-doped ZnO with remarkable photocatalytic activity using ZIF-8 as a precursor[69]. Through the pyrolysis of ZIF-8(x)@NH_2-MIL-125, which was created by embedding a MOF in another MOF, Wang et al. were able to successfully create TiO_2 containing carbon and demonstrated its exceptional catalytic activity[70]. Yingming Wang and his team also work on C-doped ZnO based MOF, which has improved photocatalytic activity [71].

It's an easy way to produce oxides with MOF as a precursor. Additionally, it has not been reported that the composite of TiO_2 and C-doped ZnO can enhance the efficiency of electron-hole separation and their photocatalytic activity. In the past few years, a significant amount of research has been done on the synthesis of semiconductor@MOF heterojunction. Harmful dyes can interact with the photocatalyst on a wide surface area of MOFs, which enriches the dyes because of this, a semiconductor@MOF heterojunction with outstanding purification capabilities low-concentration dyes in wastewater is produced by combining adsorption and photocatalysis[72]. Despite the fact that semiconductor@MOF effectively blends photocatalysis with adsorption, there are still significant problems that require attention. Among them are the following: The photocatalyst's catalytic capacity per unit mass is influenced by the amount of the metal oxide (MOF) present in the shell. Additionally, the MOF in the shell has an effect on the semiconductor's light contact efficiency. Lastly, certain MOFs and semiconductors contain heavy metals, which can lead to secondary pollution in treated water bodies[73]. Thus, further optimization is required.

2.6. MOF-on-MOF Heterojunctions for Photocatalysis

MOF@MOF heterojunctions are used in a wide range of applications, including adsorption and separation, organic and photocatalysis, electrochemical catalysis, and sensing identification (including electrical and biosensing) [21]. Regarding adsorption, Kitagawa et al. synthesized the core-shell heterojunction using a straightforward solvent synthesis technique. The shell skeleton showed size selectivity because of its small pore size, whereas the core skeleton's enormous pore size allowed for significant storage capacity. The size screening effect of 1@2 allowed for the selective capture of cetane in the 1:1 combination of cetane/isocetane [74]. In the area of photocatalysis, Liu et al. used the site-specific epitaxial growth approach to develop MIL-125@ZIF-8. Superoxide radical photocatalytic degradation of orange II was produced using internal MIL-125 as a photocatalyst. However, the positively charged ZIF-8 outside of MIL-125 decreased its negative surface potential, which allowed the negatively charged orange II and enriched orange II to adsorbed onto MIL-125 [75].

The internal growth approach was used in the Li et al. work to construct the Zn/Co-ZIFs@MIL-101 (Fe) photo-Fenton catalyst. The hybrid of the two polymetallic centers speed up electron-hole pair transfer in a synergistic manner, enhancing H_2O_2 activation and ultimately encouraging the very effective degradation toward RhB [76]. NH_2-MIL-125@NTU-9 was synthesized by Yu et al. to converge CO_2 to formate synthesis. NH_2-MIL-125@NTU-9 produced formate at 430 nm with a quantum efficiency (0.67%) and selectivity (94.47%) that clearly outperformed NH_2-MIL-125 (0.13 and 88.56%) and NTU-9 (0.16 and 89.26%) [77]. But since each part of the aforementioned double MOF heterojunction has a comparatively unique function, more research is needed to determine how the components work together functionally.

MOF@MOF would offer a platform for water pollution photocatalytic degradation and synergistic adsorption. Here, we have a kind of large-surface-area photocatalyst. The two MOF's recyclable and environmentally friendly components demonstrated outstanding adsorption and photocatalytic properties in addition to realizing the intended dual function synergy. The MIL-(Fe) MOF is the largest member of the MOF family and has the strongest photoactivity, stronger photocatalytic performance, and shorter band gap width [78]. The AOPs employing MIL-100(Fe) that have been explored the most extensively include Fenton-based procedures and photocatalytic oxidation. Additionally, MIL-100(Fe) has been studied in the ozonation of RhB; it exhibits some catalytic activity, albeit less than that of MIL-53(Fe) and MIL-88B (Fe). In photocatalytic treatments, various radiation sources (UV-C, white light, visible light and natural sunshine) were used. Given that MIL-100(Fe) has been reported to have strong photocatalytic activity in the visible spectrum, this makes it noteworthy [79, 80].Within the various semiconducting and photo-responsive MOFs, MIL-53(Al) and MIL-100(Fe) are both chromophoric and photoresponsive. Their aminated derivatives have a lot of active sites, a lot of surface heterogeneities, sensitivity to visible light, and photo-responsive NH_2 groups. Consequently, a MOF@MOF heterojunction photocatalyst (NH_2-MIL-53(Al)@MIL-100(Fe), was developed and synthesized using a simple Precipitation method based on the previously mentioned considerations for degradation of RhB dye.

CHAPTER THREE

3. MATERIALS AND METHODOLOGY

3.1. Experimental Work Site

The sustainable synthesis of selected pristine MOFs, NH_2-MIL-53(Al)/MIL-100(Fe) heterojunctions and photocatalytic degradation of RhB experiments were conducted at Debre Berhan University, Chemistry department research laboratory. XRD and SEM analysis was determined at Adama Science and Technology University (ASTU), Material Science and Engineering and Biology department, respectively. The FT-IR and DRS-UV-vis analysis was determined at Addis Ababa Science and Technology University (AASTU).

3.2. Chemicals and Reagents

All chemicals utilized for the synthesis of NH_2-MIL-53(Al), MIL-100(Fe) and NH_2-MIL-53(Al)/MIL-100(Fe) materials are analytical grade. Iron (II) chloride tetrahydrate ($FeCl_2 \cdot 4H_2O$, Sigma Aldrich, > 97%), Aluminum trichloride hexahydrate ($AlCl_3.6H_2O$, Sigma Aldrich, > 99%), Trimesic acid (H_3BTC, Sigma Aldrich, > 99%), 2-aminoterephthalic acid (NH_2-H_2BDC, Acros Organics, 99.7%), Sodium hydroxide (NaOH, Acros Organics >98%), Ethanol (C_2H_5OH, HPLC grade), RhB dye ($C_{28}H_{31}ClN_2O_3$, Sigma Aldrich, ≥99.9%) and Deionized water.

3.3. Synthesis Procedures

3.3.1. Preparation of MIL-100(Fe) MOF

The preparation of MIL-100(Fe) was adopted from the previous reported method, [81] with some modification. Typically, 1.596 g (7.6 mmol) of H_3BTC is dissolved in 23.72 g of 1.0 M NaOH aqueous solution (22.8 mmol) in Solution 1 (pH ~ 11). 2.26 g (11.4 mmol) of $FeCl_2 \cdot 4H_2O$ is dissolved in 97.2 g of H_2O to form Solution 2 (pH ~ 2.7). Following the completion of clear solutions in both instances, Solution 1 was gradually transferred over Solution 2 under continuous stirring for 24 h at room temperature (Figure (3.1)). The pH of mixture of solution was approximately 5.2 and a molar ratio of 1.5 Fe: 1.0 H_3BTC: 3.0 NaOH: 880 H_2O. The resultant solid was recovered using centrifugation at 4000 rpm, washed by water (x3, three times) and ethanol (x2, two times) and dried at room temperature. The as-obtained sample represented by MIL-100(Fe).

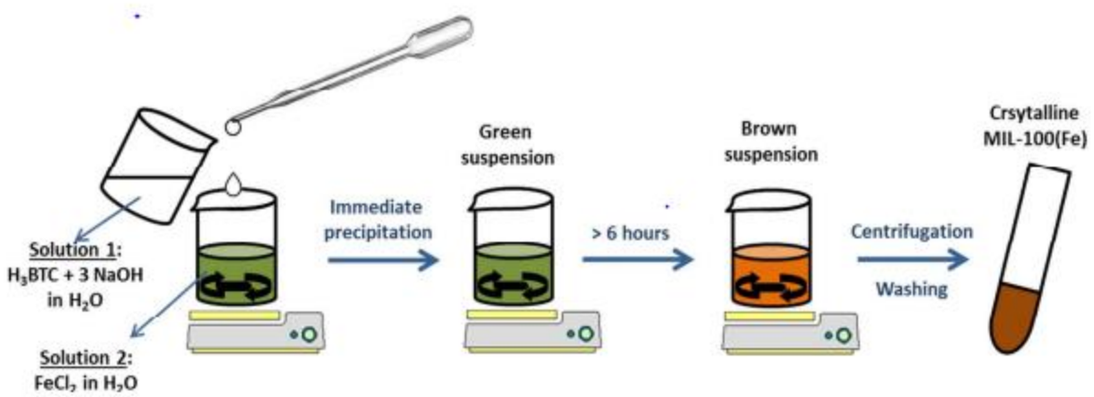

Figure 3.1. Schematic of synthesis of MIL-100(Fe) MOF via precipitation synthesis method under sustainable condition [81].

3.3.2. Preparation of NH_2-MIL-53(Al) MOF

NH_2-MIL-53(Al) was prepared by following elsewhere reported procedure[82]. Typically, 1.449 g (6.0 mmol) $AlCl_3.6H_2O$ are dissolved in 3 mL of H_2O (Solution 1) and 1.0867 g (6.0 mmol) of 2-aminoterephtalic acid (NH_2-H_2BDC in 13.05 mL 1.0 M NaOH (Solution 2). Solution 1 was added to Solution 2 under stirring after forming clear solution in both cases which resulted instantaneous yellow precipitates. The reaction was left under stirring for 24 h at room temperature. After 24 h the precipitate formed was washed and dried with the same procedure mentioned above and denoted as NH_2-MIL-53(Al).

3.3.3. Synthesis of NH_2-MIL-53(Al)/MIL-100(Fe) Heterojunctions

The NH_2-MIL-53(Al)/MIL-100(Fe)-xwt% heterojunctions (where x=1, 3, 7, and 12wt % of MIL-100(Fe)) was synthesized systematically in one step method (that is, the NH_2-MIL-53(Al) MOF was formed in the presence of MIL-100(Fe)). The required weight of MIL-100(Fe) and 0.724 g of $AlCl_3.6H_2O$ was dispersed in 30 and 1.5 mL distilled water (Solution 1 and 2), respectively. In addition, 0.544 g of 2-aminoterephtalic acid (NH_2-H_2BDC) was dissolved in 6.525 mL of 1.0 M NaOH (Solution 3). Following the completion of clear precipitate solutions in three cases Solution 2 gradually added in Solution 3, after that Solution 1 transferred immediately in the mixtures of both solutions while being stirred. After that, the reaction was left under stirring for 24 h at room temperature. After 24 h the precipitate formed was washed and dried with the same procedure mentioned above and labeled as Al/Fe-1wt%, Al/Fe-3wt%, Al/Fe-7wt% and Al/Fe-12wt%.

3.4. Characterization Techniques

The as-synthesized materials were characterized by various advanced techniques such as X-ray diffraction (XRD) using a Shimadzu XRD 7000 diffractometer equipped with scintillation detector and Cu Kα radiation (λ= 1.5418Å) to identify the crystalline structure and phase purity. The diffractograms were captured in 2θ, covering a range of 2^o to 90^o, using a scan speed of 3^o per min and under tube voltage-tube current 40 KV-40 mA. FT-IR (Perkin Elmer) spectrometry was employed to identify the surface functional groups of as-synthesized samples in the range 400-4000 cm^{-1} using the KBr pellet technique.

Scanning electron microscopy (SEM) was carried out using a Tabletop Microscope with a tungsten filament electron gun to detect the morphology of materials. UV-vis diffuse reflectance spectroscopy (DRS) measurements were run in a V-770 (JASCO) double-beam UV-vis Near-IR spectrophotometer (200-2500 nm) with scan speed 10-4000 nm per min. Collected spectra of the photocatalysts were converted to Kubelka-Munk function, F(R) versus wavelength. The photocatalytic degradation of RhB dye was determined by UV-vis spectrophotometer (Optizen POP) from 200-800 nm.

3.4. Crystallite size Measurements

The crystallite size of these samples was calculated by the Debye-Scherrer equation as follows in equation below.

$$D = 0.9\lambda / \beta cos\theta \quad (2)$$

Where D is crystallite size (nm), λ is the wavelength of Cu Kα radiation (0.15406 nm), β is the full width at half-maximum of the most intense diffraction peak (FWHM) in radians and θ is the Brag angle in radians.

3.5. Photocatalytic Degradation Efficiency Measurements

The photocatalytic efficiency of the as-synthesized samples were tested by applying irradiating visible light (85-Watt Tungsten lamp, TORCH, 85 W, 6400 K, 170-240 V/50-60 Hz) and using RhB dye as target pollutant. About 70 mg of catalyst were added into 10 parts per million (ppm) solution of pollutant. Then, the solution was stirred for 30 min in the dark to obtain adsorption-desorption equilibrium between a catalyst and pollutant. 3 mL aliquots were withdrawn at time zero. Following the achieving of equilibrium, the suspension was continuously stirred while being exposed to visible light from an 85-Watt Tungsten lamp. After that, a sample was taken from the suspension every 20 minutes for 140 minutes. Ultimately, absorbance was determined using UV-vis spectroscopy (200–800 nm) after centrifugation. The photocatalytic degradation performance (%E) of the samples under the presence and absences of light was calculated using the following [Equation (1)].

$$\%E = \frac{(A_O - A_e)}{A_O} \text{ x } 100 \quad (1)$$

Where, A_0 and Ae is the initial and final absorbance of RhB dye.

3.6. Photocatalytic mechanism of hetrojunction Measurements

To explain the photocatalytic activity the following formula was used to calculate the samples' valence band (EVB) and conduction band (ECB) potentials in relation to the normal hydrogen electrode (NHE).

$$E_{VB} = \chi - E^e + 0.5E_g \quad (3).$$

$$E_{CB} = E_{VB} - E_g \quad (4).$$

CHAPTER FOUR

4. RESULTS AND DISCUSSION

4.1. X-ray Diffraction (XRD) Analysis

X-ray diffraction was used to determine the crystal structure, crystallite size, and phase purity of as-synthesized samples. As seen in Figure 4.1(a-b) there is an XRD plot of NH_2-MIL-53(Al), MIL-100(Fe) and NH_2-MIL-53(Al)/MIL-100(Fe) heterojunctions with different weight ratio of MIL-100(Fe) contents (1, 3, 7, and 12 wt%) denoted as Al/Fe-1wt%, Al/Fe-3wt%, Al/Fe-7wt% and Al-Fe-12wt%, respectively. The XRD pattern of the NH_2-MIL-53(Al) sample (below) is depicted in Figure 4.1(a), which shows the characteristic diffraction peaks at 2θ values of 8.6^o, 10.4^o, 15^o, 17.4^o and 26.4^o corresponding to (101), (200), (011), (202) and (020) crystal planes. In which, it matches well with the simulated XRD patterns described in the literature [83]. Furthermore, the XRD patterns of as-synthesized MIL-100(Fe) sample matched exactly with the simulated data, showing comparable peaks at $2\theta = 4.0^o$, 6.2^o, 9.3^o, 10.2^o, 10.9^o, 12.5^o, 18.4^o, 20.1^o, 25.3^o, and 28.1^o[84]. The excellent agreement between the simulated and experimental XRD patterns, confirms the successful synthesis of the desired NH_2-MIL-53(Al) and MIL-100(Fe) MOFs with high quality crystalline nature.

In Figure 4.1(b) shows the XRD patterns of heterojunctions also confirmed the successful synthesis of NH_2-MIL-53(Al)/MIL-100(Fe) structure. The diffraction peaks of NH_2-MIL-53(Al)/MIL-100(Fe) heterojunction shows the characteristic peaks of the individual components. On the other hand, as the composition of MIL-100(Fe) ratio increases, the intensity of the diffraction peak at 10.2^o and 20.1^o observed, confirming the efficient loading of MIL-100(Fe).

In addition, the observed shift and broadening of the XRD peaks suggested a synergistic interaction between the two components in the MOF-on-MOF heterojunctions. This was most likely due to interfacial effects, lattice distortions, and potential alterations in overall crystallinity brought about by the formation of the heterojunction. These findings demonstrate how well the synthesis approach worked successfully to bring the NH_2-MIL-53(Al) and MIL-100(Fe) components together.

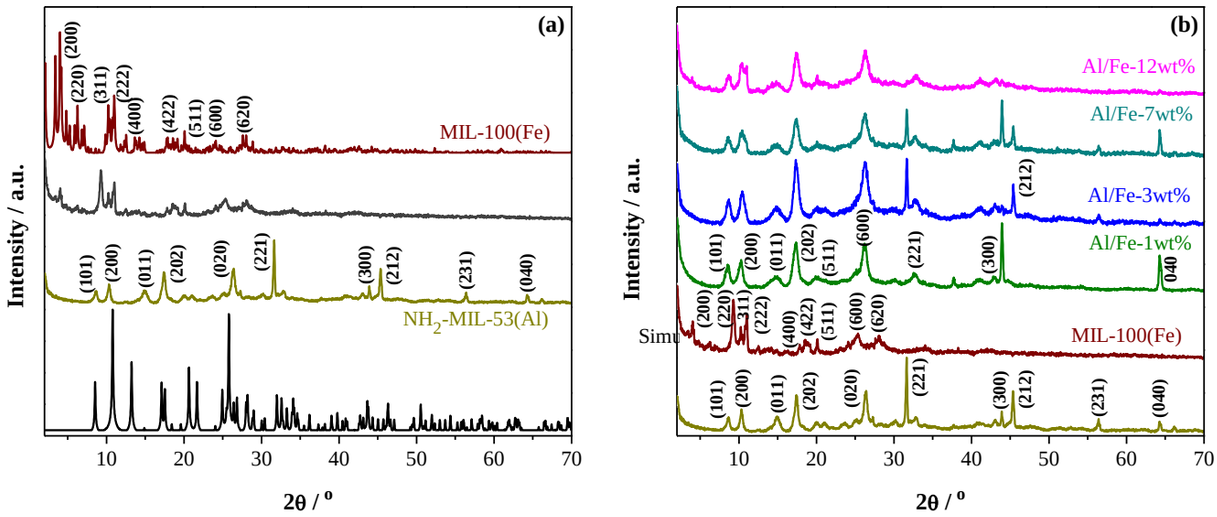

Figure 4.1. XRD patterns of (a) a simulated NH_2-MIL-53(Al) (black line) and MIL-100(Fe) (dark gray) and as-prepared NH_2-MIL-53(Al) (dark yellow) and MIL-100(Fe) at room temperature (wine) and (b) as-obtained NH_2-MIL-53(Al) (dark yellow), MIL-100(Fe) (wine), the heterojunction Al/Fe-1wt% (olive), Al/Fe-3wt% (blue), Al/Fe-7wt% (dark cyan) and Al/Fe-12wt% (magenta) samples.

The crystallite size of these samples was calculated by the Debye-Scherrer equation as follows [85]. As shown in table 4.1, the crystalline size of the nanocomposite materials is lower than that of the pristine MOF materials. This may result from interfacial effects that can limit the formation of large, well-defined crystals as well as defects caused by the presence of two MOF components in the composite [86]. This implies that, in comparison to pristine MOFs, the photocatalytic performance of MOF-on-MOF nanocomposite might be improved. As the catalyst's size lowers, the active sites and interfacial charge carrier transfer rates are improved, resulting in increased and/ or boosted photocatalytic activity.

Table 4.1. The calculated crystallite size of as-synthesized samples.

Sample	Average Crystallite Size (nm)
NH_2-MIL-53(Al)	31.6
MIL-100(Fe)	15.9
Al/Fe-1wt%	11.8
Al/Fe-3wt%	13.0
Al/Fe-7wt%	13.3
Al/Fe-12wt%	8.9

4.2. Fourier Transform Infrared (FT-IR) Spectroscopy Analysis

In order to examine the functional group and verify the bond interaction between surface functional groups, the FT-IR technique is used in this investigation. As the Figure 4.2 shows, as-prepared NH_2-MIL-53(Al) has peaks at 1600–1650 cm^{-1} which belongs to the fundamental amine (-NH_2) groups bending and stretching vibrations. The peaks at the 1257 cm^{-1} correlate to C-H bond, while peaks at 1394 cm^{-1} and 1590 cm^{-1} correspond to the carboxylic acid

functionalities of Al-coordination and organic linker structure of 2-aminoterephtalic acid, respectively. Furthermore, the peaks in the range of 500–800 cm^{-1} are indicative of the stretching vibration of metal-oxygen (Al-O), which fits along with the previously published literature [87]. In MIL-100(Fe), the carboxylic groups (C-O) bond was identified as the source of the peak at 1619 cm^{-1}. The symmetrical and asymmetrical vibrational band features of the -O-C-O- group, can be related to the sharp bands at 1442 cm^{-1} and 1371 cm^{-1}, respectively. While the distinctive peaks at 754 cm^{-1} corresponds to the C-H bending vibrations of benzene, which is consistent with the earlier published literature [84].

In FTIR spectra of NH_2-MIL-53(Al)/MIL-100(Fe) heterojunctions, the combination of distinctive features of NH_2-MIL-53(Al) and MIL-100(Fe) is displayed in the FTIR spectrum (Figure 4.2). The characteristic peaks of individual components are clearly observed in the FT-IR spectrum of NH_2-MIL-53(Al)/MIL-100(Fe) heterojunction, which exhibiting a significant vibration band at 1400−1700 cm^{-1}. The peak at 707 cm^{-1} and 1443 cm^{-1} is the distinctive peak of MIL-100(Fe). Additionally, bands in the 800-1000 cm^{-1} range imply that MIL-100(Fe) MOF co-exists with as-synthesized NH_2-MIL-53(Al)/MIL-100(Fe) heterojunctions and it also verify the successful synthesis of pristine MOFs and effective formation of heterojunction NH_2-MIL-53(Al)/MIL-100(Fe).

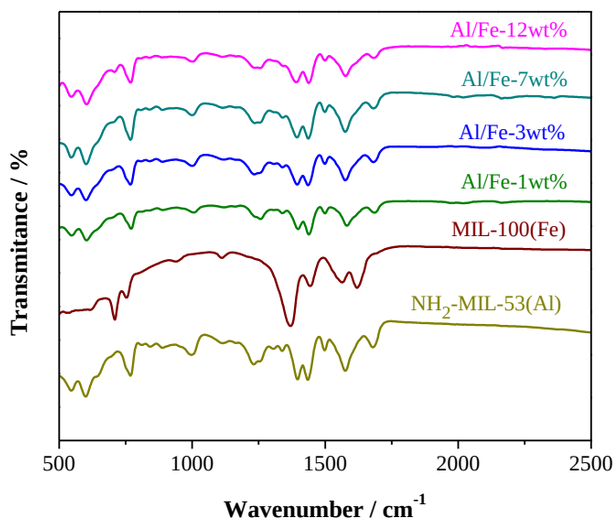

Figure 4.2. FT-IR spectra of as-prepared NH2-MIL-53(Al) (dark yellow), MIL-100(Fe) (wine), the hetrojunction Al/Fe-1wt%. (olive), Al/Fe-3wt% (blue), Al/Fe-7wt%. (dark cyan) and Al/Fe-12wt% (magenta) samples.

4.3. Scanning Electron Microscopy (SEM) Analysis

The morphologies of the as-prepared NH_2-MIL-53(Al), MIL-100(Fe), and NH_2-MIL-53(Al)/MIL-100(Fe) heterojunctions were examined using the SEM. As shown in Figure 4.3 (a) the SEM image of NH_2-MIL-53(Al) sample has uniform irregular shape distribution under micro scale level [88]. Figure 4.3(b-c) displays the SEM images of MIL-100(Fe) highly porosity and interconnected appearance with micro scale level. The sample exhibits an assembly of uniformly sized irregularly shaped particles with various diameters. The bigger structures in these particles appear to be formed from smaller crystallites that have aggregated together.

The apparent gaps and cavities between the linked particles indicate the porous character of the material. Figure 4.3(d) displays the SEM image of NH_2-MIL-53(Al)/MIL-100 (Fe) heterojunction (Al/Fe-1wt%), which confirms that the two individual component structures are intimately integrated due to different brightness indicates different composition as the images were collected with a backscattering detector.

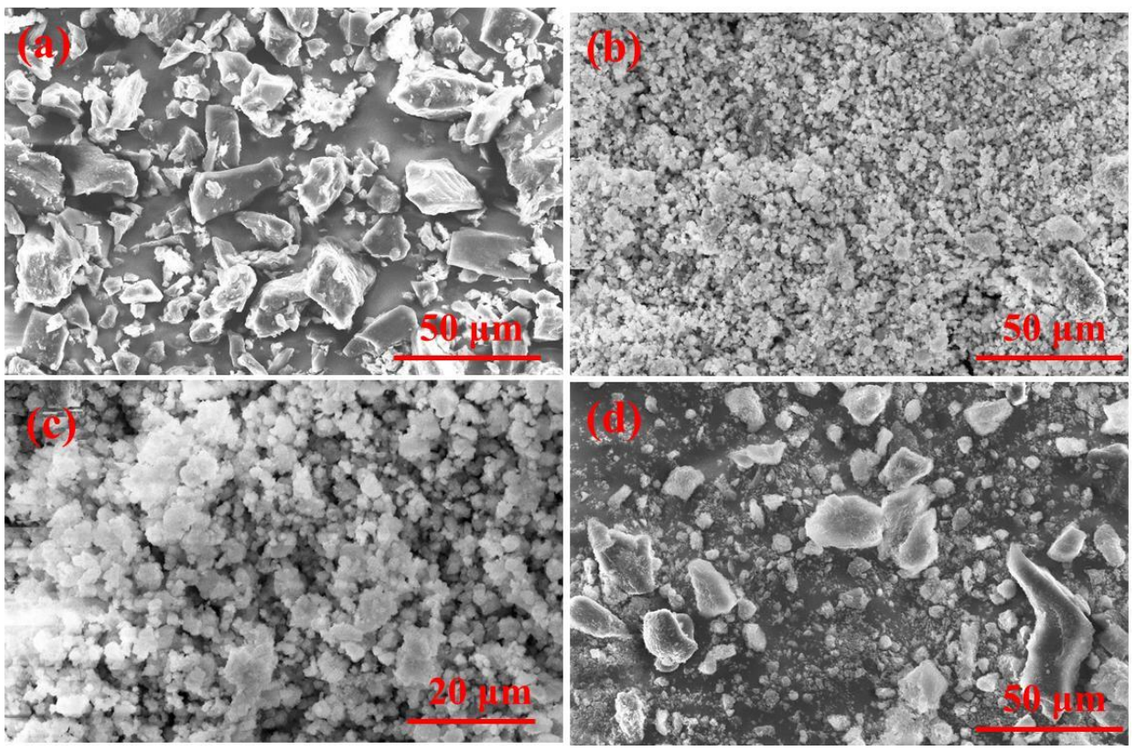

Figure 4. 3. SEM images of as-synthesized (a) NH_2-MIL-53(Al), (b-c) MIL-100(Fe) and (d) Al/Fe-1wt% hetrojunction materials.

4.4. DRS-UV-vis Spectrophotometer Analysis

The optical properties of pristine and heterojunction materials have been determined using UV-vis-spectrometer. The absorption edge of NH_2-MIL-53(Al) and MIL-100(Fe) MOFs is around 463 nm and 557 nm, respectively (Figure 4.4(a)), which confirm that they might be highly visible light driven active photocatalysts and absorb the irradiated visible light.

The heterojunctions absorption peak increases significantly, and the absorption edge shifts toward the longer wavelength region, suggesting that the addition of MIL-100(Fe) successfully broadens the composite's absorption range and enhances its optical sensitivity.

In addition, the heterojunctions of Al/Fe-1wt%, Al/Fe-3wt%, Al/Fe-7wt% and Al/Fe-12wt% have an absorption edge of around 510 nm, 589 nm, 588 nm and 579 nm, respectively, suggesting the photocatalysts absorbed more visible light due to photoactive nature of the materials. This kind of analysis is evident in a number of studies [53, 54]. The DRS-UV-vis spectroscopy was used to determine the optical band gap energy (Eg) of the as-obtained samples, which estimated by standard techniques using the plot of F(R) *vs.* wavelength given in Figure 4.4(a) either to $(F(R)h\nu)^{1/2}$ *vs.* photon energy E (in eV) shown in Figure 4.4(b) or to $(F(R)h\nu)^2$ *vs.* E (in eV) shown in Figure 4.4(c). Figure 4.4 (b-c) displays the extrapolation result of Tauc plots in the form of direct and indirect band gap of samples. Considering that $F(R)h\nu = A(h\nu - Eg)^{n/2}$, where F(R) is the Kubelka-Munk (K-M) function, h the plank's constant, ν the light frequency, A

is a constant, Eg represents the band gap and n is determined by the type of optical transition of a photocatalyst (n value is 1 for direct transition and 4 for an indirect photocatalyst), Eg can be estimated graphically as shown in both Figure 4.4(b-c).

The estimated band gap (Eg) values were demonstrated in Table 4.2. NH_2-MIL-53(Al) relatively wide direct band gap (2.76 eV) than other samples, while MIL-100(Fe) act as photo-sensitizer due to narrow indirect Eg (2.4 eV) and the indirect Eg of heterojunction of Al/Fe-1wt% (2.7 eV), Al/Fe-3wt% (2.31 eV), Al/Fe-7wt% (2.15 eV) and Al/Fe-12wt% (2.44 eV). Additionally the Eg is lowered to smaller values through coupling of MIL-100(Fe), proving that heterojunction formation effectively, which leads to narrows the Eg and facilitates visible light absorption [89]. This phenomenon confirms red shift, as the result of effective coupling of individual components, most likely due to of an electron-hole transition that occurs between the as-synthesized composite material components, which enhances the material's efficiency for target RhB dye detection and photocatalytic degradation as well [90].

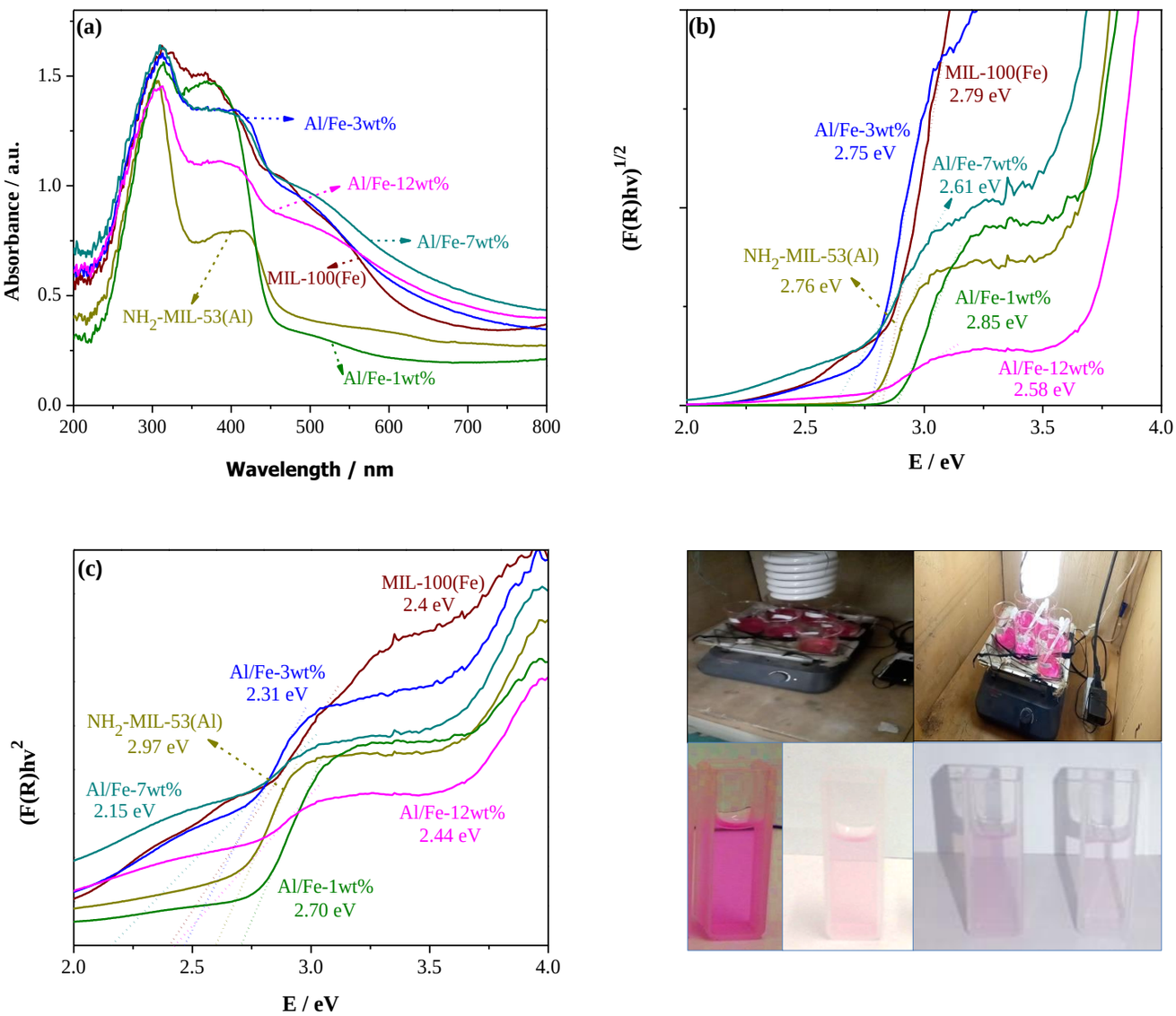

Figure 4.4. (a) DRS-UV-vis spectra, (b-c) Tauc plot of $(F(R)hv)^{1/2}$ *versus* hv and $(F(R)hv)^2$ *versus* hv, respectively, of pristine NH_2-MIL-53(Al) (dark yellow line) and MIL-100(Fe) (wine) and the heterojunction of Al/Fe-1wt%. (olive), Al/Fe-3wt%. (blue), Al/Fe-7wt%. (dark cyan) and Al/Fe-12wt% (magenta) and (d) real images of expirmental set up and RhB dye colour change**.**

Table 4.1. The absorption edge and so-estimated band gap value of samples.

Sample	Absorption edge (nm) (estimated from Figure 4.4a)	Band gap (eV) (estimated from Figure 4.4b)	Band gap (eV) (estimated from Figure 4.4c)
NH_2-MIL-53(Al)	463	2.76	2.97
MIL-100(Fe)	557	2.79	2.4
Al/Fe-1wt%	510	2.85	2.7
Al/Fe-3wt%	589	2.75	2.31
Al/Fe-7wt%	588	2.61	2.15
Al/Fe-12wt%	579	2.58	2.44

4.5. Photocatalytic Activity

Prior to evaluating the photocatalytic activity of the as-prepared catalysts for photocatalysis, the heterojunction Al/Fe-7wt% was used to optimize the operational parameters (including, the solution of pH, the catalyst dose, irradiation time and initial RhB dye concentration) in the photocatalytic process.

4.5.1. pH optimization

pH affects the properties of dyes as well as the chemical pathways that might cause dye degradation, such as attacks by hydroxyl radicals, direct oxidation by positive holes, and direct reduction by electrons in the conduction band, as a result, finding the optimum pH is neccesary step in photocatalytic activity [91]. The RhB dye's pH was adjusted using 0.1M HCl and 0.1M NaOH solution for acidic and basic media, respectively, in order to examine the impacts of pH on the degradation performance. The pH ajusts from pH value of 2 to12. As the, Figure (4.5) below,demonstrates there is an optimal balance at pH 6, indicating the higher photocatalytic degradation performance.

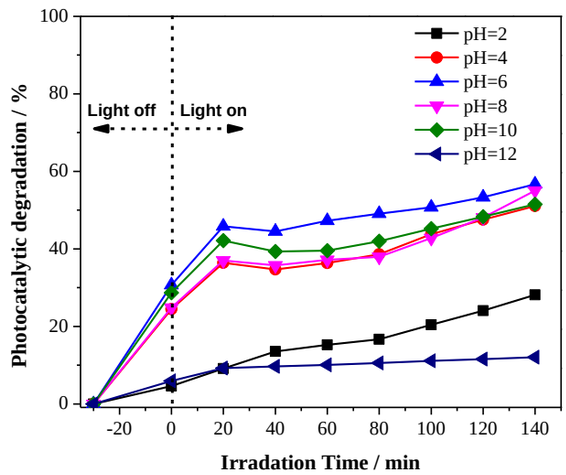

Figure 4.5. Plots of photocatalytic degradation *versus* reaction time in the RhB degradation at different pH of the reaction medium with heterojunction Al/Fe-7wt%. Reaction conditions: tungsten lamp as a visible light source (TORCH,85 W,6400 K, 170-240 V/50-60Hz) the distance between the top of the reactor and the lamp was 11 cm, catalyst loading of 30 mg , RhB Concentration of 10 mg L^{-1} and 140 minutes of reaction time.

4.5.2. Initial dye concentration

In photocatalytic dye degradation, optimizing RhB dye concentration is a necessary stage as it directly impacts the process's overall effectiveness. The initial concentration of dye influences both adsorption and light penetration by balancing the number of dye molecules to degraded and

the accessible active sites on the photocatalyst [92].Thus having the optimal initial dye concentration can aid in boosting the dye removal capacity.

As shown in Figure 4.6, the RhB dye concentration of (10, 20, 30, 40 and 50 ppm) studied preliminary, thus, at an initial concentration of 10 ppm, the as-synthesized Al/Fe-7w% heterojunction material displayed higher degrading efficiency and effectively removed a substantial amount of dye from the solution. However, the selected heterojunction catalytic effectiveness started to decrease at the higher initial dye concentrations of 20 to 50 ppm. This was probably because there was less mass transfer and less light penetration in the process [93]. Consequently, 10 ppm is considered to be the ideal initial dye concentration, as this is where the material can best utilize its photocatalytic properties to remove dye effectively without diminishing its overall effectiveness.

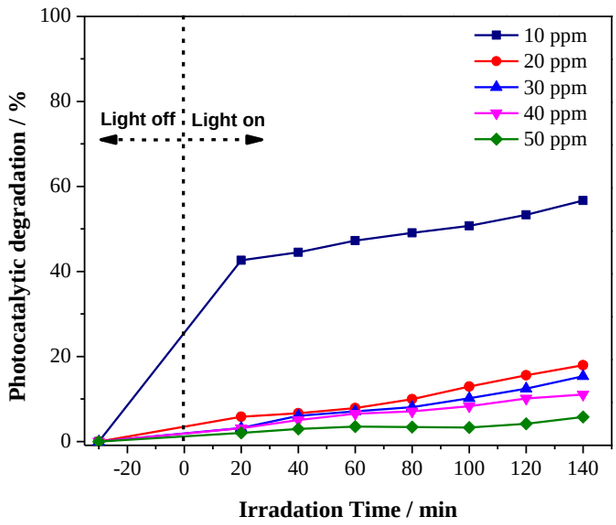

Figure 4. 6. Plots of photocatalytic degradation versus reaction time in optimizing the impact of Initial RhB dye concentration with selected heterojunction Al/Fe-7wt%. Reaction conditions: tungsten lamp as a visible light source (TORCH,85 W,6400 K, 170-240 V/50-60Hz) the distance between the top of the reactor and the lamp was 11 cm, catalyst loading of 30 mg , pH=6 and 140 minutes of reaction time.

4.5.3. Catalyst loading

Photocatalyst loading is the quantity of photocatalyst material that is present in the reaction system and expressed as the mass of the reaction medium. Since, it determines the number of active sites that will be available in the reaction, optimization of photocatalyst loading is one of the most crucial steps in photocatalytic activity [94]. As Figure (4.7) below, shows the effect of catalyst amount (20, 30, 40, 50, 60, 70, 80 and 90 mg) studied, also as a reference blank (no catalyst) condition included. As a result, a catalyst loading of 70 mg photocatalyst performed better than the other photocatalyst loadings.

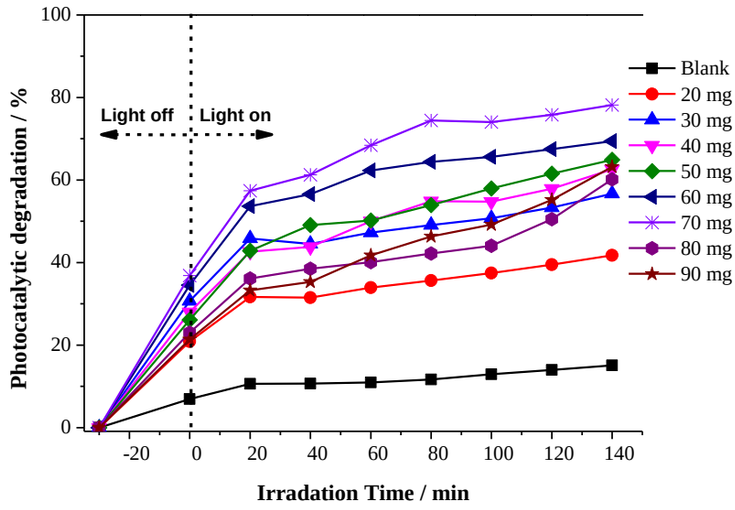

Figure 4.7. Plots of photocatalytic activity in the RhB removal at different catalyst loading using different amount of Al/Fe-7wt% heterojunction. Reaction conditions: tungsten lamp as a visible light source (TORCH,85 W,6400 K, 170-240 V/50-60Hz) the distance between the top of thereactor and the lamp was 11 cm, RhB Concentration of 10 mg L-1, pH=6 and 140 minutes of reaction time.

4.6. Comparison of Photocatalysts

After the optimization parameter has been fulfilled, the photocatalytic efficiency of our pristine nanomaterial's and heterojunction was evaluated by comparing their photocatalytic performance under visible light, as shown in Figure 4.7. Based on that, under visible light irradiation, the pristine NH_2-MIL-53(Al) MOF exhibits comparatively low photocatalytic activity (78% after 140 min) most likely it is because of high electron-hole recombination. However, MIL-100(Fe) MOF are visible light responsive and exhibits good photocatalytic activity (93% after 140 minutes) than NH_2-MIL-53(Al) but less photocatalytic decolorization of RhB compared to Al/Fe-1wt% (95% in 140 minutes) under visible light irradiation due to high recombination rate of charge carriers in MIL-100(Fe). It goes saying that the couplings between NH_2-MIL-53(Al) and MIL-100(Fe) were intended to facilitate the transmission and separation of electrons and holes, to reduce the rate of recombination.

As a result, the photocatalytic activities of as-obtained heterojunction photocatalysts (Al/Fe-3wt% Al/Fe-7wt% and Al/Fe-12wt%) are comparatively good (90%, 81%, and 78% after 140 minutes, respectively) (Figure 4.8). While still less than Al/Fe-1wt% heterojunction and pristine MIL-100(Fe), this could be because adding more MIL-100(Fe) to the heterojunction NH_2-MIL-53(Al)/MIL-100(Fe) reduces the photocatalytic performance by reducing light harvesting efficiency and the recombination of charge carriers issue [95]. Such unquestionable synergistic effect is also found in the heterojunction based Al/Fe-1wt%, which exhibit excellent photocatalytic activity 95% in 140 minutes. Large contact area at the interface between the NH_2-MIL-53(Al) and MIL-100(Fe) could be conducive to this [96].

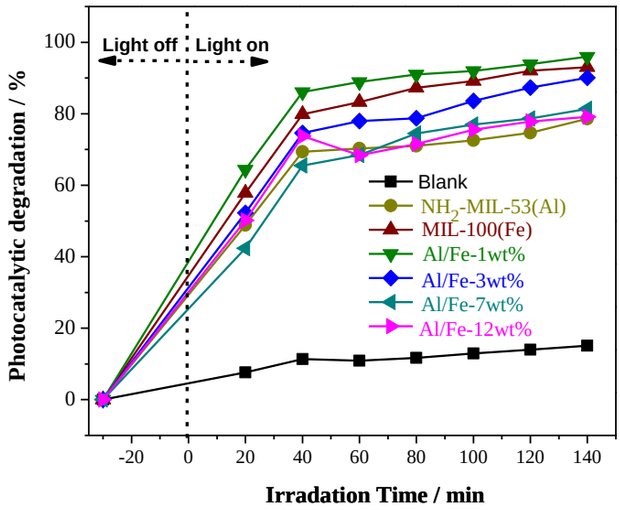

Figure 4.8. Plots of photocatalytic degradation versus reaction time in the RhB degradation in the presence of different photocatalysts. Reaction conditions: tungsten lamp as a visible light source (TORCH,85 W,6400 K, 170-240 V/50-60Hz) the distance between the top of the reactor and the lamp was 11 cm, catalyst loading of 70 mg , RhB Concentration of 10 mg L-1, pH=6 and 140 minutes of reaction time.

Additional tests with Al/Fe-1wt% photocatalyst were conducted in three scenarios to compare the light effect: in natural sunlight/ solar (outdoor system), with tungsten lamp as a visible light source (indoor system) and without catalyst (blank). The as-synthesized heterojunction material exceptional performance under natural solar light/outdoor system circumstances is demonstrated by Figure 4.9, which shows how our heterojunction photocatalyst outperforms compared to the other reaction conditions, this may be due to the intensity difference of the light.

As-prepared Al/Fe-1wt% photocatalyst in outdoor condition, exhibiting 99.5% photocatalytic activity in just 80 minutes this is could be due to the outside environment allows the catalyst to fully conquer the improved light harvesting, charge separation and catalytic active site availability which drives from the synergistic effect of both NH_2-MIL-53(Al) and MIL-100(Fe) MOFs and the strengthen the light intensity, thus leading to highest photocatalytic efficiency [97]. Furthermore, the material exhibits a 90% photocatalytic activity in 80 minutes under indoor lighting conditions, demonstrating the catalyst's efficient degradation ability of RhB dye under artificial light (Figure 4.9). Although, relatively less effective than the natural solar light reaction condition. Conversely, there is also Blank reaction condition, in which no catalyst is used and there is essentially no dye degradation in the absence of the Al/Fe-1wt% photocatalyst. This is an excellent instance or condition to confirm the catalytic activity of the as-synthesized NH_2-MIL-53(Al)/MIL-100(Fe) heterojunction material is the reason for the RhB dye degradation that was observed.

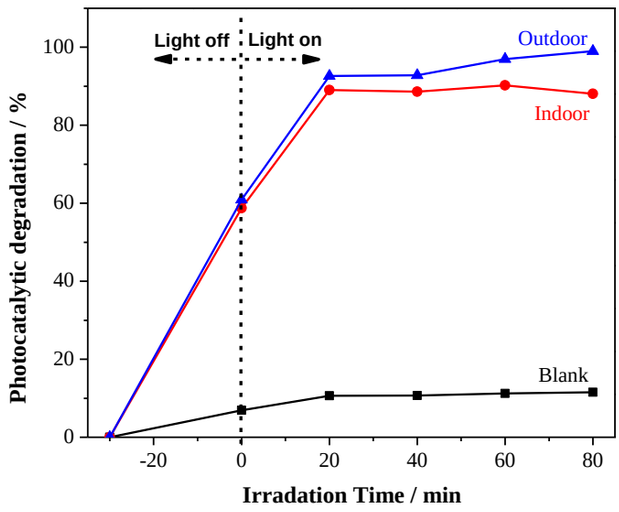

Figure 4.9. Comparison the photocatalytic performance for RhB dye degradation under indoor (visible), outdoor (solar) and without catalyst (blank) conditions. Reaction conditions: tungsten lamp as a visible light source (TORCH,85 W,6400 K, 170-240 V/50-60Hz) the distance between the top of the reactor and the lamp was 11 cm, catalyst loading of 70 mg , RhB Concentration of 10 mg L-1, pH=6 and 80 minutes of reaction time.

4.7. Photocatalytic Mechanism

4.7.1. Scavengers effect

Throughout the photocatalytic process, essential active species are produced, including superoxide anion radicals, hydroxyl radicals, and photogenerated electrons and holes from light irradiation[98]. To clarify the characteristics of the active species super oxide radicals ($\bullet O_2^-$) or electrons, hydroxyl radicals (•OH, photo-oxidation of water), and holes (h^+) which are entrapped in the Al/Fe-1wt% heterojunction throughout the photocatalytic operation and the reaction mechanism, scavengers such as, 10 mL of 0.1 M sodium sulfate (Na_2SO_4) [99], methanol (CH_3OH) [98], and sodium hydrogen carbonate ($NaHCO_3$) [100] were used, respectively.

As (Figure 4.10) shows the introduction of methanol resulted in an increase in the photocatalytic degradation of RhB (95.8% when absent and 99.0% when present). This showed that ($\bullet OH^-$) radicals have less effect in the degradation of RhB dye. However, sodium hydrogen carbonate and sodium sulfate, significantly affect photoactivity, bringing the efficiency down to 84.5% and 90.6%, respectively. This suggests that the main active species in the RhB degradation are both super oxide radicals ($\bullet O_2^-$) or electrons and holes [101, 102].

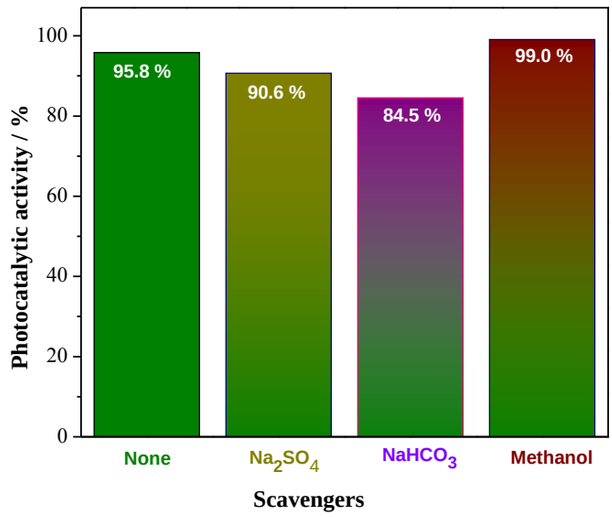

Figure 4.10. Effect of trapping agent in the photodegradation of RhB by Al-Fe-1wt% heterojunction under visible light irradiation. Reaction conditions: tungsten lamp as a visible light source (TORCH,85 W,6400 K, 170-240 V/50-60Hz) the distance between the top of the reactor and the lamp was 11 cm, catalyst loading of 70 mg , RhB Concentration of 10 mg L-1, pH=6 and 80 minutes of reaction time. The color of the columns is a mixture between the olive, violet and wine.

4.7.2. Photocatalytic mechanism of hetrojunction

To explain the photocatalytic activity the following formula was used to calculate the samples' valence band (EVB) and conduction band (ECB) potentials in relation to the normal hydrogen electrode (NHE).

Where the absolute electronegativity of the MOFs; NH_2-MIL-53(Al) = 5.3 eV [103] and MIL-100(Fe) = 5.1 eV [104].

E_g is the bandgap energy, while E^e, the energy of free electrons on the hydrogen scale, has a value of 4.5 eV. According to the findings of the UV-vis study, NH_2-MIL-53(Al) had band potentials of +2.3 and -0.7 eV, while MIL-100(Fe) had band potentials of +1.8 and -0.6 eV. As a result, Equations (3) and (4), respectively, were used to compute the E_{VB} and E_{CB} values for NH_2-MIL-53(Al) and MIL-100(Fe).

Table 4.3. Band Gap, Conduction Band, Valance Band, and Electronegativity Positions of NH2-MIL-53(Al) and MIL-100(Fe) Photocatalysts on NHE.

Photocatalyst	χ (eV)	E_g (eV)	E_{CB} (eV)	E_{VB} (eV)
MIL-100(Fe)	5.1	2.4	-0.6	+1.8
NH_2-MIL-53(Al)	5.3	2.97	-0.7	+2.3

The NH_2-MIL-53(Al)/MIL-100(Fe) heterojunction's band alignment is essential to comprehending the charge separation and transfer mechanisms that improve photocatalytic activity. The band potentials of NH_2-MIL-53(Al) and MIL-100(Fe) provided +1.8 and -0.6 eV, respectively, based on the band potential values that were provided.

In MIL-100(Fe) and NH_2-MIL-53(Al), electron-hole pairs are generated under light irradiation. The photogenerated electrons in the conduction band of MIL-100(Fe) (-0.6 eV) transfer to the

conduction band of NH_2-MIL-53(Al) (-0.7 eV), while the photogenerated holes in the valence band of NH_2-MIL-53(Al) (+2.3 eV) transfer to the valence band of MIL-100(Fe) (+1.8 eV) due to the favorable band alignment. By preventing electron-hole pair recombination, this charge separation and transfer improve photocatalytic efficiency. The NH_2-MIL-53(Al)/MIL-100(Fe) heterojunction system's total photocatalytic efficiency for the degradation of Rhodamine B dye is improved by the synergistic effect of these charge separation and transfer processes, hole-mediated oxidation, and superoxide radical formation.

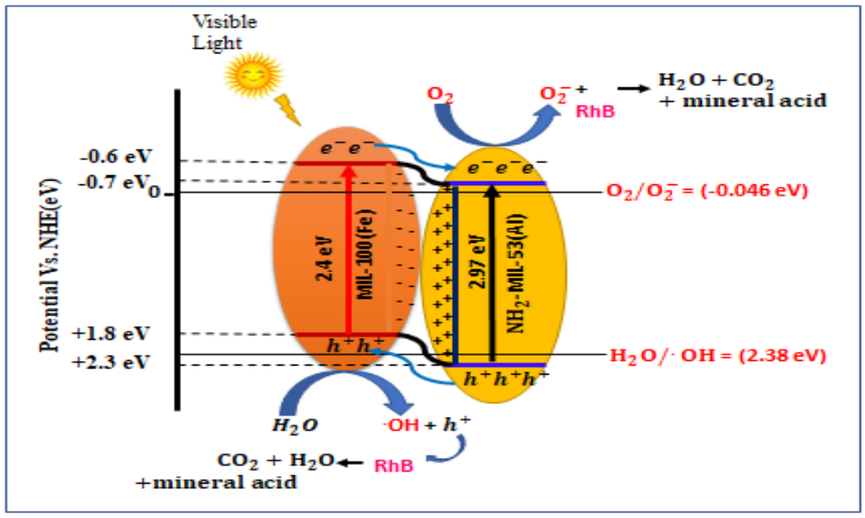

Figure 4.11. The plausible diagram of photogenerated electron-hole transfer mechanisms in NH2-MIL-53(Al)/MIL-100(Fe) Heterojunction under visible irradiation.

4.7.3. Reusability of photocatalyst

During four successive cycles, the photocatalytic and reusablity of this catalyst were examined. It is noteworthy that the photocatalyst activity remains significant after four cycles (91.4% vs. 83% of second and fourth cycles) and is remarkably fascinating in the second cycle with an activity of 91.4% (Figure 4.11).

It needs to be mentioned that throughout the washing and separating processes between the several cycles, there was a loss of about 2 mg of catalyst weight. Despite this loss after four cycles, the catalytic performance is still highly significant. This result showed that the NH_2-MIL-53(Al)/MIL-100(Fe) crystal and chemical structure exhibited good stability.

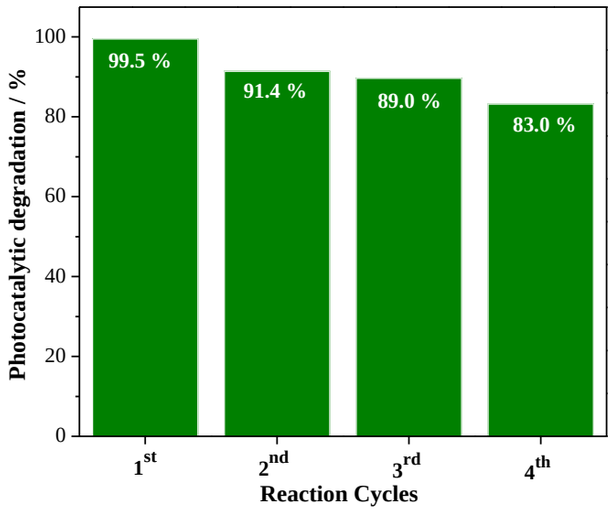

Figure 4.12. RhB degradation by the Al/Fe-1wt%. for different consecutive cycles. Reaction conditions: natural sunlight as alight source, RhB concentration of 10 mg L-1, 60 minutes of reaction time, and pH =6.

5. CONCLUSIONS

In order to remove RhB dye, the target MOF-on-MOF heterojunction was successfully synthesized by coupling MIL-100(Fe) MOF with NH_2-MIL-53(Al) under sustainable approach, which confirmed by the various physicochemical characterization techniques. The heterojunction significantly increases charges transfer and the catalyst's electron-hole separation efficiency, allowing more e- and h^+ to be used for redox reactions than pristine MOFs. This leads to a notable improvement in the catalyst's photocatalytic efficiency for RhB degradation under visible light. Furthermore, by improving the catalyst's adsorption capabilities, the MOF-on-MOF heterojunctions can offer benefit for later photocatalytic degradation under indoor and outdoor systems. At an optimal Al/Fe-1wt% ratio over 80% of the RhB dye can degraded in 60 minutes and over 95% of the dye can be degraded after 140 minutes of photocatalyst. Aditionaly, the study of the RhB photodegradation mechanism through the use of the scavengers to trap the active site has demonestrated that superoxide radical (O_2^-) and hole (h^+) plays the critical role in the RhB photodegradation process, with h^+ having the most significant impact. Finally, Al/Fe-1wt% displayed remarkable recyclability, retaining a high photocatalytic degradation efficency of 83.0% even after four cycles of activity. This work offers a novel approach to the efficient degradation of RhB dye with MOF-on-MOF heterojunctions like NH_2-MIL-(53)/MIL-100(Fe) under visible and solar conditions.

5.1. Recommendation and Future Works

In order to prevent environmental pollution and ensure the safety of society, it is imperative that undesirable and harmful materials be removed from wastewater and industrial effluents before they are released into the environment. In this work, the heterojunction NH_2-MIL-(53)/MIL-100(Fe) have promising photocatalytic degradation of RhB dyes under visible and solar light driven systems. We recommend the use of MOFs and MOF-on-MOF heterojunctions for the future work. MOFs have shown great promise as materials for a variety of uses, such as environmental remediation, energy storage, gas separation, and catalysis. Especially, the development of MOF-on-MOF heterostructures, which have the potential to reveal synergistic effects and increased functions in addition with their unthinkable properties, is a promising avenue for future growth in MOF research. MOF-on-MOF hetrojunction are composed of two or more different MOF materials arranged in a layered or hierarchical way. By combining the beneficial qualities of several MOFs, this innovative architecture can increase performance and diversify the range of state-of-the-art applications.

REFERENCES

1. Sohrabnezhad, S. and S. Moghadamy, *Zinc oxide nanorods incorporated magnetic isoreticular metal–organic framework for photodegradation of dyes.* Journal of Molecular Structure, 2022. **1247**: p. 131353.
2. He, S., et al., *Femtosecond time-resolved diffuse reflectance study on facet engineered charge‐carrier dynamics in Ag3PO4 for antibiotics photodegradation.* Applied Catalysis b: Environmental, 2021. **281**: p. 119479.
3. Forgacs, E., T. Cserháti, and G. Oros, *Removal of synthetic dyes from wastewaters: a review.* Environment international, 2004. **30**(7): p. 953-971.
4. Gnanasekaran, G., et al., *Efficient removal of anionic, cationic textile dyes and salt mixture using a novel CS/MIL-100 (Fe) based nanofiltration membrane.* Chemosphere, 2021. **284**: p. 131244.
5. Mahmoodi, N.M., et al., *Metal-organic framework (MIL-100 (Fe)): Synthesis, detailed photocatalytic dye degradation ability in colored textile wastewater and recycling.* Materials Research Bulletin, 2018. **100**: p. 357-366.
6. Coha, M., et al., *Advanced oxidation processes in the removal of organic substances from produced water: Potential, configurations, and research needs.* Chemical Engineering Journal, 2021. **414**: p. 128668.
7. Hejazi, R., et al., *Fabrication of novel type visible-light-driven TiO2@ MIL-100 (Fe) microspheres with high photocatalytic performance for removal of organic pollutants.* Journal of Photochemistry and Photobiology A: Chemistry, 2020. **400**: p. 112644.
8. Chen, Y., et al., *Recent progress on the removal of antibiotic pollutants using photocatalytic oxidation process.* Critical Reviews in Environmental Science and Technology, 2022. **52**(8): p. 1401-1448.
9. Sepehrmansourie, H., et al., *A MOF-on-MOF strategy to construct double Z-scheme heterojunction for high-performance photocatalytic degradation.* Applied Catalysis B: Environmental, 2023. **321**: p. 122082.
10. Wang, C.-C., et al., *Photocatalytic organic pollutants degradation in metal–organic frameworks.* Energy & Environmental Science, 2014. **7**(9): p. 2831-2867.
11. Mondal, K. and A. Sharma, *Photocatalytic oxidation of pollutant dyes in wastewater by TiO2 and ZnO nano-materials–a mini-review.* nanoscience & technology for mankind, 2014: p. 36-72.
12. Hao, F., Z.Y. Yan, and X.P. Yan, *Recent advances in research on the effect of physicochemical properties on the cytotoxicity of metal–organic frameworks.* Small Science, 2022. **2**(9): p. 2200044.
13. Wang, Y., et al., *Metal organic framework-derived C-doped ZnO/TiO2 nanocomposite catalysts for enhanced photodegradation of Rhodamine B.* Journal of Colloid and Interface Science, 2021. **599**: p. 566-576.

14. He, Y., et al., *Modified MIL-100 (Fe) for enhanced photocatalytic degradation of tetracycline under visible-light irradiation.* Journal of colloid and interface science, 2020. **574**: p. 364-376.
15. Zhang, C.-F., et al., *A novel magnetic recyclable photocatalyst based on a core–shell metal–organic framework Fe 3 O 4@ MIL-100 (Fe) for the decolorization of methylene blue dye.* Journal of Materials Chemistry A, 2013. **1**(45): p. 14329-14334.
16. Huang, J., et al., *Facile synthesis of N-doped TiO2 nanoparticles caged in MIL-100 (Fe) for photocatalytic degradation of organic dyes under visible light irradiation.* Journal of environmental chemical engineering, 2017. **5**(3): p. 2579-2585.
17. Zhao, C., et al., *Bifunctional Bi12O17Cl2/MIL-100 (Fe) composites toward photocatalytic Cr (VI) sequestration and activation of persulfate for bisphenol A degradation.* Science of the Total Environment, 2021. **752**: p. 141901.
18. Ahmadijokani, F., et al., *Coordination chemistry of metal–organic frameworks: Detection, adsorption, and photodegradation of tetracycline antibiotics and beyond.* Coordination Chemistry Reviews, 2022. **464**: p. 214562.
19. Ramezanalizadeh, H. and F. Manteghi, *Synthesis of a novel MOF/CuWO4 heterostructure for efficient photocatalytic degradation and removal of water pollutants.* Journal of Cleaner Production, 2018. **172**: p. 2655-2666.
20. Wu, M.-X., et al., *Core–shell MOFs@ MOFs: diverse designability and enhanced selectivity.* ACS Applied Materials & Interfaces, 2020. **12**(49): p. 54285-54305.
21. Liu, C., et al., *MOF-on-MOF hybrids: Synthesis and applications.* Coordination Chemistry Reviews, 2021. **432**: p. 213743.
22. Jin, Y., et al., *Modular construction of an MIL-101 (Fe)@ MIL-100 (Fe) dual-compartment nanoreactor and its boosted photocatalytic activity toward tetracycline.* ACS Applied Materials & Interfaces, 2022. **14**(42): p. 48285-48295.
23. He, X., et al., *Self-assembled synthesis of recyclable g-C3N4/NH2-MIL-53 (Fe) aerogel for enhanced photocatalytic degradation of organic pollutants.* Journal of Alloys and Compounds, 2023. **946**: p. 169391.
24. Chiu, N.-C., et al., *Designing dual-functional metal–organic frameworks for photocatalysis.* Chemistry of Materials, 2022. **34**(19): p. 8798-8807.
25. Vijayan, K. and S. Vijayachamundeeswari, *Improving the multifunctional attributes and photocatalytic dye degradation of MB and RhB dye–A comparative scrutiny.* Inorganic Chemistry Communications, 2022. **144**: p. 109940.
26. Kaur, K. and R. Jindal, *Synergistic effect of organic-inorganic hybrid nanocomposite ion exchanger on photocatalytic degradation of Rhodamine-B dye and heavy metal ion removal from industrial effluents.* Journal of environmental chemical engineering, 2018. **6**(6): p. 7091-7101.
27. Pavithra, K.G. and V. Jaikumar, *Removal of colorants from wastewater: A review on sources and treatment strategies.* Journal of Industrial and Engineering Chemistry, 2019. **75**: p. 1-19.

28. Rodriguez-Narvaez, O.M., et al., *Treatment technologies for emerging contaminants in water: A review.* Chemical Engineering Journal, 2017. **323**: p. 361-380.
29. Jung, C.-R., Y.-T. Lin, and B.-F. Hwang, *Ozone, particulate matter, and newly diagnosed Alzheimer's disease: a population-based cohort study in Taiwan.* Journal of Alzheimer's Disease, 2015. **44**(2): p. 573-584.
30. Huang, J., et al., *Ionic liquid assisted hydrothermal preparation of TiO_2 with largely enhanced photocatalytic performance originated from effective separation of photoinduced carriers.* Journal of Physics and Chemistry of Solids, 2020. **139**: p. 109323.
31. Chen, J., et al., *Nanostructured BiVO4 derived from Bi-MOF for enhanced visible-light photodegradation.* Chemical Research in Chinese Universities, 2020. **36**(1): p. 120-126.
32. Younis, S.A., et al., *Metal-organic framework as a photocatalyst: Progress in modulation strategies and environmental/energy applications.* Progress in Energy and Combustion Science, 2020. **81**: p. 100870.
33. Qu, L.-L., et al., *Iron (iii)-based metal–organic frameworks as oxygen-evolving photocatalysts for water oxidation.* Sustainable Energy & Fuels, 2018. **2**(9): p. 2109-2114.
34. Van Seventer, J.M. and N.S. Hochberg, *Principles of infectious diseases: transmission, diagnosis, prevention, and control.* International encyclopedia of public health, 2017: p. 22.
35. Jalali, S., et al., *One step integration of plasmonic Ag_2CrO_4/Ag/AgCl into HKUST-1-MOF as novel visible-light driven photocatalyst for highly efficient degradation of mixture dyes pollutants: Its photocatalytic mechanism and modeling.* Polyhedron, 2019. **166**: p. 217-225.
36. Parveen, S. and A. Malviya, *Analytical Review on Membrane Water Filter using Different Materials to Prevent Microbial Activities.* Journal of Pure & Applied Microbiology, 2022. **16**(4).
37. Zou, L., et al., *Fabrication and dye removal performance of magnetic $CuFe_2O_4$@ CeO_2 nanofibers.* Applied Surface Science, 2015. **332**: p. 674-681.
38. Güy, N. and M. Özacar, *Ag/Ag_2CrO_4 nanoparticles modified on ZnO nanorods as an efficient plasmonic photocatalyst under visible light.* Journal of Photochemistry and Photobiology A: Chemistry, 2019. **370**: p. 1-11.
39. Bidu, J.M., et al., *Current status of textile wastewater management practices and effluent characteristics in Tanzania.* Water science and Technology, 2021. **83**(10): p. 2363-2376.
40. Kausar, A., et al., *Preparation and characterization of chitosan/clay composite for direct Rose FRN dye removal from aqueous media: comparison of linear and non-linear regression methods.* Journal of Materials Research and Technology, 2019. **8**(1): p. 1161-1174.
41. Soriano, J.B., et al., *Global, regional, and national deaths, prevalence, disability-adjusted life years, and years lived with disability for chronic obstructive pulmonary disease and asthma, 1990–2015: a systematic analysis for the Global Burden of Disease Study 2015.* The Lancet Respiratory Medicine, 2017. **5**(9): p. 691-706.

42. Saratale, R.G., et al., *A critical review on anaerobic digestion of microalgae and macroalgae and co-digestion of biomass for enhanced methane generation.* Bioresource technology, 2018. **262**: p. 319-332.
43. Hutagalung, S., I. Muchlis, and K. Khotimah. *Textile wastewater treatment using advanced oxidation process (AOP)*. in *IOP conference series: materials science and engineering*. 2020. IOP Publishing.
44. Hemashenpagam, N. and S. Selvajeyanthi, *Textile Dyes and Their Effect on Human Beings*, in *Nanohybrid Materials for Treatment of Textiles Dyes*. 2023, Springer. p. 41-60.
45. Lotfi, S., et al., *Recent progress on the synthesis, morphology and photocatalytic dye degradation of BiVO4 photocatalysts: A review.* Catalysis Reviews, 2024. **66**(1): p. 214-258.
46. Pascariu, P., et al., *Photocatalytic activity of ZnO–SnO_2 ceramic nanofibers for RhB dye degradation: experimental design, modeling, and process optimization.* physica status solidi (b), 2019. **256**(5): p. 1800474.
47. Tahir, M.B., et al., *WO nanostructures-based photocatalyst approach towards degradation of RhB dye.* Journal of Inorganic and Organometallic Polymers and Materials, 2018. **28**: p. 1107-1113.
48. Samer, M., *Biological and chemical wastewater treatment processes.* Wastewater treatment engineering, 2015. **150**(10.5772): p. 61250.
49. Zhao, C., et al., *Facile synthesis of Fe_3O_4/MIL-101 nanocomposite as an efficient heterogeneous catalyst for degradation of pollutants in Fenton-like system.* RSC advances, 2017. **7**(39): p. 24453-24461.
50. Jia, G., et al., *1D alignment of ZnO@ ZIF-8/67 nanorod arrays for visible-light-driven photoelectrochemical water splitting.* Applied Surface Science, 2018. **448**: p. 254-260.
51. Nahar, S., et al., *Photocatalytic degradation of organic pollutants over visible light active plasmonic Ag nanoparticle loaded Ag_2SO3 photocatalysts.* Journal of Photochemistry and Photobiology A: Chemistry, 2019. **375**: p. 191-200.
52. Hao, M., et al., *Enhanced visible light photocatalytic activity in AgI/BiOCOOH composite.* Advanced Powder Technology, 2019. **30**(1): p. 111-119.
53. Yang, C.-L. and J. McGarrahan, *Electrochemical coagulation for textile effluent decolorization.* Journal of hazardous materials, 2005. **127**(1-3): p. 40-47.
54. Adnan, O., et al., *A novel biocoagulant agent from mushroom chitosan as water and wastewater therapy.* Environmental Science and Pollution Research, 2017. **24**: p. 20104-20112.
55. Zhang, M.-h., et al., *A review on Fenton process for organic wastewater treatment based on optimization perspective.* Science of the Total Environment, 2019. **670**: p. 110-121.
56. Andreozzi, R., M. Canterino, and R. Marotta, *Fe (III) homogeneous photocatalysis for the removal of 1, 2-dichlorobenzene in aqueous solution by means UV lamp and solar light.* Water research, 2006. **40**(20): p. 3785-3792.

57. Pandis, P.K., et al., *Key points of advanced oxidation processes (AOPs) for wastewater, organic pollutants and pharmaceutical waste treatment: A mini review.* ChemEngineering, 2022. **6**(1): p. 8.
58. Li, S., et al., *Photocatalytic degradation of hazardous organic pollutants in water by Fe-MOFs and their composites: A review.* Journal of Environmental Chemical Engineering, 2021. **9**(5): p. 105967.
59. Saravanan, R., F. Gracia, and A. Stephen, *Basic principles, mechanism, and challenges of photocatalysis.* Nanocomposites for visible light-induced photocatalysis, 2017: p. 19-40.
60. Lamba, R., et al., *Enhanced visible light driven photocatalytic application of Ag_2O decorated ZnO nanorods heterostructures.* Separation and Purification Technology, 2017. **183**: p. 341-349.
61. Saravanan, R.R., F. Gracia, and A. Stephen. *Chapter 2 Basic Principles , Mechanism , and Challenges of Photocatalysis*. 2017.
62. Zhao, Y., Y. Li, and L. Sun, *Recent advances in photocatalytic decomposition of water and pollutants for sustainable application.* Chemosphere, 2021. **276**: p. 130201.
63. Diercks, C.S. and O.M. Yaghi, *The atom, the molecule, and the covalent organic framework.* Science, 2017. **355**(6328): p. eaal1585.
64. Yaghi, O.M., *Reticular Chemistry Construction, Properties, and Precision Reactions of Frameworks*. 2016, ACS Publications. p. 15507-15509.
65. Nguyen, H.L., et al., *A titanium–organic framework as an exemplar of combining the chemistry of metal–and covalent–organic frameworks.* Journal of the American Chemical Society, 2016. **138**(13): p. 4330-4333.
66. Zhou, H.-C., J.R. Long, and O.M. Yaghi, *Introduction to metal–organic frameworks*. 2012, ACS Publications. p. 673-674.
67. Titirici, M.-M. and P.Á. Szilágyi, *Hydroxide ion-conducting metal–organic frameworks for anion-exchange membrane applications.* Materials Advances, 2022. **3**(24): p. 8815-8829.
68. Khan, M.S., et al., *A Review of Metal-Organic Framework (MOF) Materials as an Effective Photocatalyst for Degradation of Organic Pollutants.* Nanoscale Advances, 2023.
69. Feng, Y., et al., *ZIF-8 derived porous N-doped ZnO with enhanced visible light-driven photocatalytic activity.* Journal of Physics and Chemistry of Solids, 2017. **102**: p. 110-114.
70. Bhadra, B.N., et al., *TiO_2-containing carbon derived from a metal–organic framework composite: a highly active catalyst for oxidative desulfurization.* ACS applied materials & interfaces, 2017. **9**(36): p. 31192-31202.
71. Wang, Y., et al., *Microwave hydrothermally synthesized metal–organic framework-5 derived C-doped ZnO with enhanced photocatalytic degradation of rhodamine B.* Langmuir, 2020. **36**(33): p. 9658-9667.

72. Sheng, H., et al., *Urchin-inspired TiO_2@ MIL-101 double-shell hollow particles: adsorption and highly efficient photocatalytic degradation of hydrogen sulfide.* Chemistry of Materials, 2017. **29**(13): p. 5612-5616.
73. Melillo, A., et al., *MOF-on-MOF composites with UiO-66-based materials as photocatalysts for the overall water splitting under sunlight irradiation.* Energy & Fuels, 2023. **37**(7): p. 5457-5468.
74. Hirai, K., et al., *Sequential functionalization of porous coordination polymer crystals.* Angewandte Chemie (International ed. in English), 2011. **50**(35): p. 8057-8061.
75. Liu, C., et al., *Site-specific growth of MOF-on-MOF heterostructures with controllable nano-architectures: beyond the combination of MOF analogues.* Chemical science, 2020. **11**(14): p. 3680-3686.
76. Li, Y., et al., *Zn/Co-ZIFs@ MIL-101 (Fe) metal–organic frameworks are effective photo-Fenton catalysts for RhB removal.* Separation and Purification Technology, 2022. **293**: p. 121099.
77. Yu, Y., et al., *Solar-driven CO_2 conversion promoted by MOF− on− MOF homophase junction.* Catalysis Communications, 2021. **150**: p. 106270.
78. Yang, S., et al., *Materials Institute Lavoisier (MIL) based materials for photocatalytic applications.* Coordination Chemistry Reviews, 2021. **438**: p. 213874.
79. Chávez, A., et al., *Critical aspects of the stability and catalytic activity of MIL-100 (Fe) in different advanced oxidation processes.* Separation and Purification Technology, 2021. **255**: p. 117660.
80. Humayun, M., et al., *Enhanced photocatalytic performance of novel MIL53Sr metal-organic framework (MOF) for RhB dye degradation and H_2 evolution by coupling MIL53Fe.* Solar Energy, 2021. **215**: p. 121-130.
81. Guesh, K., et al., *Sustainable preparation of MIL-100 (Fe) and its photocatalytic behavior in the degradation of methyl orange in water.* Crystal Growth & Design, 2017. **17**(4): p. 1806-1813.
82. Habib, N.R., et al., *The effect of non-ionic surfactants on the sustainable synthesis of selected MOFs.* Catalysis Today, 2022. **390**: p. 316-325.
83. Yang, Y., et al., *NH_2-MIL-53 (Al) nanocrystals anchored on the surface of RGO hollow spheres and its visible light degradation of methylene blue.* Materials Letters, 2017. **197**: p. 17-20.
84. Nehra, M., et al., *Metal organic frameworks MIL-100 (Fe) as an efficient adsorptive material for phosphate management.* Environmental research, 2019. **169**: p. 229-236.
85. Fu, D., et al., *Fabrication of α-FeOOH decorated graphene oxide-carbon nanotubes aerogel and its application in adsorption of arsenic species.* Journal of colloid and interface science, 2017. **505**: p. 105-114.
86. Shan, Y., et al., *Synthesis and catalytic application of defective MOF materials.* Cell Reports Physical Science, 2023. **4**(3).

87. Zhao, H., et al., *Gear-shaped mesoporous NH_2-MIL-53 (Al)/CdS PN heterojunctions as efficient visible-light-driven photocatalysts.* Applied Catalysis B: Environmental, 2021. **291**: p. 120106.
88. Guan, Y., et al., *Water-based preparation of nano-sized NH_2-MIL-53 (Al) frameworks for enhanced dye removal.* Inorganica Chimica Acta, 2019. **484**: p. 180-184.
89. Qin, D., et al., *One-pot calcination synthesis of Cd0. 5Zn0. 5S/g-C_3N_4 photocatalyst with a step-scheme heterojunction structure.* Journal of Materials Science & Technology, 2020. **56**: p. 206-215.
90. Navarathna, C.M., et al., *Rhodamine B adsorptive removal and photocatalytic degradation on MIL-53-Fe MOF/magnetic magnetite/biochar composites.* Journal of Inorganic and Organometallic Polymers and Materials, 2020. **30**: p. 214-229.
91. Alkaim, A., et al., *Effect of pH on adsorption and photocatalytic degradation efficiency of different catalysts on removal of methylene blue.* Asian Journal of Chemistry, 2014. **26**(24): p. 8445.
92. Camarillo, R. and J. Rincon, *Photocatalytic discoloration of dyes: relation between effect of operating parameters and dye structure.* Chemical engineering & technology, 2011. **34**(10): p. 1675-1684.
93. Wang, W.-Y. and Y. Ku, *Effect of solution pH on the adsorption and photocatalytic reaction behaviors of dyes using TiO_2 and Nafion-coated TiO2.* Colloids and Surfaces A: Physicochemical and Engineering Aspects, 2007. **302**(1-3): p. 261-268.
94. Yunus, N., et al. *Effect of catalyst loading on photocatalytic degradation of phenol by using N, S Co-doped TiO_2.* in *IOP Conference Series: Materials Science and Engineering*. 2017. IOP Publishing.
95. Yassin, J.M., A.M. Taddesse, and M. Sánchez-Sánchez, *Sustainable synthesis of a new semiamorphous Ti-BDC MOF material and the photocatalytic performance of its ternary composites with Ag_3PO_4 and g-C_3N_4.* Applied Surface Science, 2022. **578**: p. 151996.
96. Chen, Y., et al., *Preparation of CdS/g-C_3N_4/MOF composite with enhanced visible-light photocatalytic activity for dye degradation.* Journal of Solid State Chemistry, 2019. **274**: p. 32-39.
97. Abdollahi, B., et al., *Cu (BDC) metal–organic framework (MOF)-based Ag_2CrO_4 heterostructure with enhanced solar-light degradation of organic dyes.* Inorganic Chemistry Communications, 2022. **138**: p. 109236.
98. Schneider, J. and D.W. Bahnemann, *Undesired role of sacrificial reagents in photocatalysis*. 2013, ACS Publications. p. 3479-3483.
99. Selvam, K. and M. Swaminathan, *One-pot photocatalytic synthesis of quinaldines from nitroarenes with Au loaded TiO_2 nanoparticles.* Catalysis Communications, 2011. **12**(6): p. 389-393.
100. Taddesse, A.M., et al., *Polyaniline supported CdS/CeO_2/Ag_3PO_4 nanocomposite: An "AB" type tandem nn heterojunctions with enhanced photocatalytic activity.* Journal of Photochemistry and Photobiology A: Chemistry, 2021. **406**: p. 113005.

101. Zhang, Z., et al., *Electrospun nanofibers of ZnO− SnO_2 heterojunction with high photocatalytic activity.* The Journal of Physical Chemistry C, 2010. **114**(17): p. 7920-7925.

102. Rajeshwar, K., et al., *Heterogeneous photocatalytic treatment of organic dyes in air and aqueous media.* Journal of photochemistry and photobiology C: photochemistry reviews, 2008. **9**(4): p. 171-192.

103. Habib, Nejat Redwan, Abi Tadesse, Manuel Sánchez-Sánchez, Raquel Sainz, and Isabel Diaz. "Copper-Loaded Sustainable Mofs as Photocatalysts for Dye Removal." Available at SSRN 4806558.

104. Yang, Jia, Xiaojun Niu, Shaorong An, Weiyi Chen, Jie Wang, and Wei Liu. "Facile synthesis of Bi_2MO_6–MIL-100 (Fe) metal–organic framework composites with enhanced photocatalytic performance." RSC advances 7, no. 5 (2017): 2943-2952.

.